Chapter 3
Control of Grid Connected Converter (GCC) Under Grid Voltage Disturbances

Marek Jasiński, Grzegorz Wrona and Szymon Piasecki

Abstract In this chapter operation of a reliable control method of a Grid Connected Converter (GCC) under grid voltage disturbances is presented. As a GCC authors understand power electronic AC-DC converter with AC side filter and DC-link capacitor operating as an interface between the electrical grid and Active Loads (AL). At the beginning short introduction to selected grid voltage disturbances is given. Afterwards, the chosen modeling approach of a GCC is discussed and the example of passive components calculation are provided. In the next sections a brief review of a basic GCC control methods is described. A control method: Direct Power Control with Space Vector Modulation (DPC-SVM) is chosen for further development process. For the basic scheme of DPC-SVM special control modules for voltage dips and higher harmonics compensation are presented. Due to the development of new control modules and its integration with the classical DPC-SVM a new reliable (robust to selected grid voltage disturbances such as dips, higher harmonics) control method is proposed: Robust Direct Power Control with Space Vector Modulation (RDPC-SVM). The term "*robust*" in the name of proposed control refers to the fact that the RDPC-SVM method is expected to operate in an uncertain environment with respect to the system dynamics. This new control method can assure sinusoidal like and balanced AC current in extremely distorted grid voltage. Based on the case study from series 5–400 kVA of Voltage Source Converters (VSCs) it was verified that the control dynamic and features of the RDPC-SVM fulfill requirements of sinusoidal and balanced currents under uncertain grid voltage distortions. Moreover, the quality

M. Jasiński (✉) · G. Wrona · S. Piasecki
Institute of Control and Industrial Electronics, Warsaw University of Technology, Warsaw, Poland
e-mail: marek.jasinski@ee.pw.edu.plmja@isep.pw.edu.pl

G. Wrona
e-mail: grzegorz.wrona@ee.pw.edu.pl

S. Piasecki
e-mail: szymon.piasecki@ee.pw.edu.pl

T. Orłowska-Kowalska et al. (eds.), *Advanced and Intelligent Control in Power Electronics and Drives*, Studies in Computational Intelligence 531,
DOI: 10.1007/978-3-319-03401-0_3,

of current and power is significantly improved in comparison to classical methods. Hence, the negative impact of the GCC on the grid voltage (through its inner impendence) is significantly reduced i.e.: lower Total Harmonics Distortion (THD) factor of a grid current, control of active and reactive power flow assure good quality of integration with a grid even in case of increased impedance within operation limits.

1 Grid Voltage Disturbances: Introduction

In this chapter, based on particular example, is presented how to design and control the Grid Connected Converter (GCC) under distorted grid voltage conditions to keep the currents always as close to sinusoidal shape as possible (low THD) and balanced. GCC is defined as grid friendly, modern power electronic converter operating as an interface between the grid and distributed sources. It gives also possibility of energy saving because provides inverting mode useful in renewable energy application and in case of Adjustable Speed Drives (ASD) regenerative braking with energy saving capability [1]. Due to, systematical cost reduction of the semiconductor devices and digital control platforms, GCCs are serially produced from range of few kVA up to MVA.

There are a lot of different aspects related with power quality (especially with grid voltage disturbances), it is impossible to address all of them in one short chapter. In this section only short introduction to the problem of the grid voltage disturbances is given. Therefore, for more information the best source of knowledge related to power quality issues are standards, recommendations [2–18], and excellent references like Bollen, Strzelecki, Hanzelka [2, 19].

There are several regulations (standards, scientific papers, and recommendations) with information about power quality, reliability and allowed voltage disturbances that have to be taken into account while power electronics GCC is going to be connected to the utility grid.

One of them is SEMI F47-0706 standard completely rewritten in 2006. This standard is devoted to semiconductors industry. It takes into account power quality aspects, especially voltage sags (dips) [2–19]. The main aim of the document is to give information about voltage dips immunity of a device needed in semiconductor processing, metrology, and automated test equipment. There are some requirements and recommendation according to immunity of the device in case of using it under voltage dips in semiconductor mass production process. It helps to make a trade of decision between voltage dips immunity and higher costs of power electronics devices. The SEMI F47 is related to another standards: a IEC 61000-4-11 [11], related to dips phenomena. This is convenient because helps to meet both standards under one similar assumptions and grid voltage dips electronics devices immunity tests. However, it should be noted that the IEC 61000 (EN 61000) (developed by national experts) standards are unceasing updated and changed. There is also

CENELEC EN 50160 [5] standard which has been also updated very often during recent 10 years. At this point, some IEEE recommendations, practices and requirements i.e. IEEE 519-1992 or IEEE 1159 (developed by volunteers) has to be mentioned [3, 4]. These recommendations should also be taken into account in the development process of a GCC features. Moreover, there are also several local regulations of a grid operators so called "*grid codes*". These grid codes usually are very precise and more strict than standards as in case of Wales, Germany, Denmark [17, 20]. In a grid code detailed information about integration with local power system can be found.

Taking into account dynamic changes of the power quality requirements and development of power electronics devices it is worth to focus on control methods of power electronic converters and its reliability in case of grid voltage dips, higher harmonics etc. In the literature can be found a relations between disturbance levels [19]: immunity level, emission level, compatibility level, planning level, design level versus probability density function of equipment performance degradation. For novel, environment friendly power electronics devices requirements according to power layer and control layer should be systematically updated to fulfill standards and reduce a negative influence on supply network. It would be convenient to think about GCC hardware like about power electronics building block (PEBB) that is unified and ready for programming of different sophisticated functionalities. The software (control methods) should be designed in modular way, allows to update and add new needed/expected by customer functionalities (e.g. grid voltage dips compensations module, higher harmonics compensation module or standalone operation mode module etc.).

There are two main groups of grid voltage disturbances: dips and higher harmonics. The terminology of grid voltage disturbances in literature is not unified, therefore some clarification is needed. In North America market the term sags is understanding as:

- voltage sag depth—the value in percent of nominal voltage remaining during the sag,
- and voltage sag duration—measured in cycles or in seconds.

In case of European EN 60160 voltage dip is:

- a temporary reduction of the one RMS voltage at a Point of Common Coupling (PCC) below specified start threshold (equals to 90 % of the reference voltage),
- voltage dip duration—is a time between the instant at which the one RMS voltage in the PCC falls below the start threshold value and the instant at which the one voltage rises the end threshold (time is from 10 ms up to including 1 min),
- voltage dip residual voltage—is a minimum value of the one RMS voltage occurred during a voltage dip (expressed as a percentage of the reference voltage) [5].

Harmonics distortion is defined by a Total Harmonic Distortion (THD) factor. The THD can be also calculated in deferent ways:

- in North America up to 50th higher harmonic,
- in Europe up to 40th higher harmonics.

Both mentioned groups of grid voltage distortions are described below.

1.1 Grid Voltage Dips

Generally, dips are temporary reduction in one, two or three phases of the RMS voltage. During dips a phase shift between each phases can also be changed. Dips can be caused by intentional changing of a power system configuration or by unpredicted short circuits. Dips can occur symmetrically (voltages in each phases are equal—Fig. 1c) and asymmetrically (as presented in Fig. 1a, b).

As it was mentioned in the introduction that dips (sags) can be described in different manner like in IEEE recommendations (493-1998, 1159-1995, 1346-1998): 70 % dip from 230 V means that voltage falls to the value equals to $230\ V \times 0.7 = 161\ V$. Hence, there is a possibility to make a mistake easily, because 70 % dip can be understand that voltage RMS value falls to 30 % of nominal RMS value. To avoid confusion in the literature reader can find a recommendation that when the dip is described it is better to write: "dip to 70 % of nominal voltage" [2–4]. Fortunately, in IEC standards this problem was solved by dip definition as an actual percentage voltage falls in respect to nominal RMS voltage value [5].

To summarize, in this chapter dip will be described as RMS voltage value reduction between 90 and 1 % of declared RMS voltage value. After a short period of time (from 10 ms up to including 1 min) the RMS voltage value returns to declared RMS voltage value [5]. In Fig. 1a different types of voltage dips are presented.

Dip is quite similar to short circuit, however the voltage drop is higher than 1 % of declared value. According to the EN 50160 standard dips can be classified as [5]:

- short (below few second) and weak ($\leq$60 %),
- short (below few second) and deep ($\geq$60 %),
- long (more than few second) and weak ($\leq$60 %),
- long (more than few second) and deep ($\geq$60 %).

It has to be stressed that change in grid voltage RMS value can cause a number of problems in control of grid connected converters e.g. DC-link voltage oscillations, distortion of the phase currents (like unbalance), active and reactive powers oscillations [21].

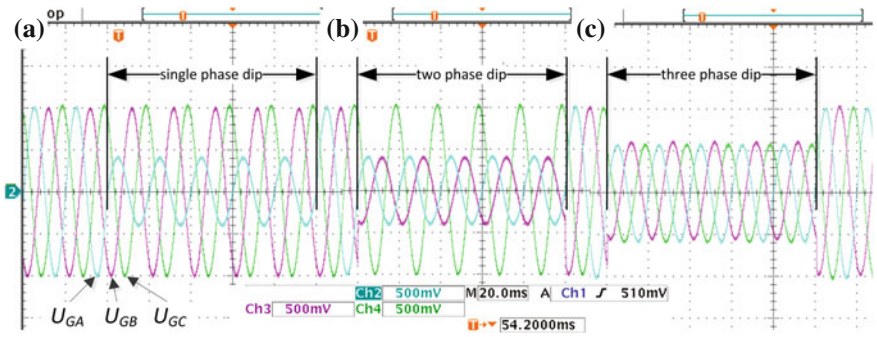

Fig. 1 Different voltage dips: **a** single-phase, **b** two-phase, **c** three-phase

1.2 Grid Voltage Harmonics

Higher harmonics are components which frequencies are being multiple of the fundamental frequency. Therefore, in Europe (50 Hz grid frequency) second harmonic frequency equals to 100 Hz, etc. Voltage harmonics are produced by nonlinear loads like: diode rectifiers, traction rectifiers, thyristor-based industrial drives etc., connected to the PCC. Because of large number of nonlinear loads the amount of higher harmonics is growing. Harmonics can cause a serious problems or even damage of electrical or electronics devices.

Several different definitions of higher harmonics distortion can be found in the literature. According to the EN 50160 standard higher harmonics are measured under normal operation conditions, during each period of week, 95 % of the 10 min mean RMS values of each individual harmonic voltage shall be less or equal to the values given in Tables 1 and 2. Note that harmonics higher than h = 25 is difficult to predict because it mainly depends on resonances. The THD factor of the grid voltage for considered voltage level (taking into account all harmonics up to 40) shall be less or equal to 8 % [5] or to 4 % [17] (taking into account all harmonics up to 50). Other recommended limit of the voltage disturbances given by IEEE 519-1992 is 5 % for the THD and below 3 % for each individual frequency. In this case the limit for individual harmonics is determined by number of loads at PCC (e.g. 10) and grid nominal voltage level (e.g. <69 kV).

Moreover, according to IEEE 519-1992 and EN 50160 the THD factor can be calculated as:

$$THD_{IEEE} = \sqrt{\frac{\sum_{h=2}^{50} U_{G(h)}^2}{U_{G(1)}^2}} 100\% \quad THD_{EN} = \sqrt{\sum_{h=2}^{40} U_{G(h)}^2} \tag{1}$$

It has to be remembered that computers and associated equipment such as programmable controllers frequently require AC sources that have voltage harmonics distortion lower than the 5 % of the THD, with the largest single harmonic

Table 1 Odd voltage harmonics in different standards and grid codes [4, 5, 17]

Odd harmonics						
Not multiples of 3			Any h of harmonics, Uh (%)	Multiples of 3		
Order h	Relative Amplitude, Uh (%)			Order h	Relative Amplitude, Uh (%)	
	EN50160	Wales	IEEE519-1992		EN50160	Wales
5	6	3	< 3	3	5	3
7	5	3	< 3	9	1.5	1.5
11	3.5	2	< 3	15	0.5	0.3
13	3	2	< 3	21	0.5	0.2
17	2	1.6	< 3			
19	1.5	1.2	< 3			
23	1.5	1.2	< 3			
25	1.5	0.7	< 3			
> 25	na	0.2 + 0.5(25/h)	< 3			

Table 2 Even voltage harmonics in different standards and grid codes [4, 5, 17]

Even harmonics			
Not multiples of 3			
Order h	Relative Amplitude, Uh (%)		
	EN50160	Wales	IEEE519-1992
2	2	1.5	< 3
4	1	1	< 3
6…24	0.5	na	< 3
6		0.5	
8		0.4	
10		0.4	
12		0.2	
> 12		0.2	

being lower than 3 % of the fundamental component. Higher levels of harmonics result in erratic, malfunctions of the equipment that can, in some cases, have serious consequences (e.g. costly brakes in mass production process) [22]. Also, instruments can be affected similarly. Perhaps the most serious malfunctions are in medical instruments. Consequently, many medical instruments are provided with special power electronics devices (line-conditioners). Here is a wide application field, mainly for AC-DC-AC converters, operating as uninterruptible power supplies systems.

Therefore, a lot of methods for elimination of harmonics distortion in the power system are developed and implemented [19, 23]. Moreover, several blackouts in recent years (USA and Canada (New York, Detroit, Toronto) in 08.2003, Russia (Moscow) in 05.2005, USA (Los Angeles) 09.2005) and in 2008, Poland (Szczecin

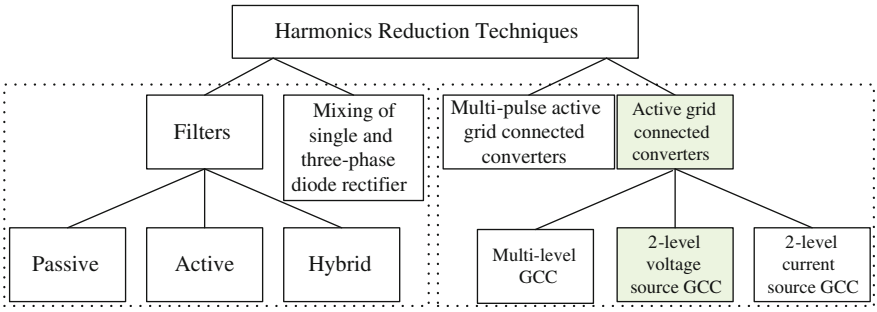

Fig. 2 Selected higher harmonics compensation method

area), shows that the power quality and reliability improvement are serious and important problems.

Methods of harmonics reduction can be divided into two main groups (Fig. 2):

- passive and active filters—harmonics reduction of the already installed non-linear loads,
- multi-pulse rectifiers and GCC—power-grid friendly converters (with limited THD index) [21].

Because the grid friendly GCC and its control methods are a scope of this chapter here it will described harmonics reduction method realized by the GCC. After modification an active filtering function can be introduced into a GCC control structure [24–28]. Moreover, the GCC can compensate current of a non-linear load connected in parallel to the PCC.

It should be stressed that in real power system a voltage is usually distorted by higher harmonics as shown in Fig. 3. This distortion has a negative impact on the grid current formed by a power electronics converter.

2 Modeling and Basic Control Methods of Grid Connected Converter

In this section mathematical modeling of the GCC is described. As can be seen from literature precise mathematical modeling of the controlled object is very important in control process [29–44]. Here we will focused on VSC modeling operating as a GCC. This description is significantly shortened but more detailed information can be found in [45–48].

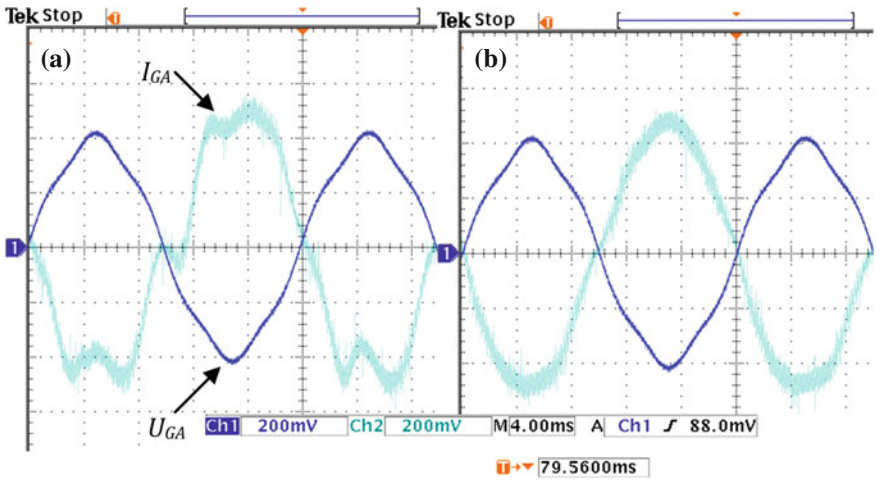

Fig. 3 Distorted grid voltage by 5th harmonic and grid current for applied control method: **a** without higher harmonics compensation, **b** with higher harmonics compensation feature

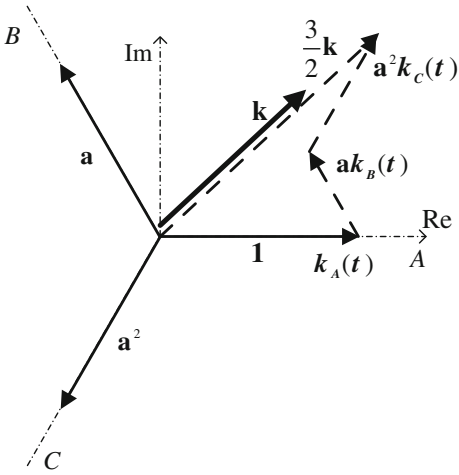

Fig. 4 Graphical representation of a Space Vector (SV) described by Eq. (2)

2.1 Space Vector Description Used in Modeling of a Voltage Source Converter

Considered, symmetric three-phase system is described by phase quantities in natural coordinate system, such as voltages, currents and fluxes or Virtual Fluxes (VF) [45, 48]. Due to Space Vector (SV) representation this system can be expressed by one SV of voltage and current respectively [49, 50]. In Fig. 4 the SV graphical representation is given.

$$\underline{\mathbf{k}} \stackrel{\text{def}}{=} \frac{2}{3}\left(k_A(t) + \boldsymbol{a}k_B(t) + \boldsymbol{a}^2 k_C(t)\right) \tag{2}$$

where 2/3 is normalization factor, $1, \boldsymbol{a} = -1/2 + j\sqrt{3}/2, \boldsymbol{a}^2 = -1/2 - j\sqrt{3}/2$ are complex unity vectors, with phase shift, $k_A(t), k_B(t), k_C(t)$ denote phase quantities in a system of natural coordinates satisfying the condition:

$$k_A(t) + k_B(t) + k_C(t) = 0 \tag{3}$$

An advantage of SV is possibility of their representation in various coordinates. Therefore, space vectors are very flexible and comfortable tool to describe a three-phase objects.

2.2 Voltage Source Converter (VSC): Basic Constrains

Let consider a 2-level VSC as presented in Fig. 5. Main circuit of the three-phase bridge converter consists of three legs with two controllable power-electronics devices (e.g. Insulated Gate Bipolar Transistors (IGBT), Metal-Oxide Semiconductor Field-Effect Transistor (MOSFET), and other transistors based on Silicon Carbide (SiC)). Under consideration in this chapter the IGBT will be selected. When transistor is in conducting mode the gate signal is "1" and when transistor is in blocking mode the gate signal is "0".

This circuit can be treated as a PEBB which may be adopted to any personal (custom) needs compatible with assumption presented in this chapter. Pre-implemented classical control method may be simple extended by additional modules to meet evolving power quality standards [51, 52].

The converter AC voltage can be obtained by eight possible switching states as shown in Fig. 6. For simplicity of the converter structure, each VSC leg is represented by an ideal switch. Six switching states construct active vectors and two switching states are related with zero vectors states. The converter AC voltage can be represented as a complex SV as follows (Fig. 7):

$$\underline{\mathbf{U}}_{c(n)} = \frac{2}{3} U_{dc} e^{j(n-1)\pi/3}, \quad n = 1, \ldots, 6 \tag{4}$$

$$\underline{\mathbf{U}}_{c(n)} = 0, \quad n = 0, 7 \tag{5}$$

Active states correspond to phase voltage equal $1/3$ and $2/3$ of the DC voltage U_{DC}. Zero vectors apply zero voltage to the converter AC side (all AC side phases are connected to "+" (1, 1, 1) or "−" (0, 0, 0) DC bar). Hereafter, please consider the case that a VSC is connected to the grid and operates as a GCC. As it was mentioned the GCC can be described in different coordinate system by SV equations. Basic scheme of the GCC with small AC passive filter (usually *LCL* or

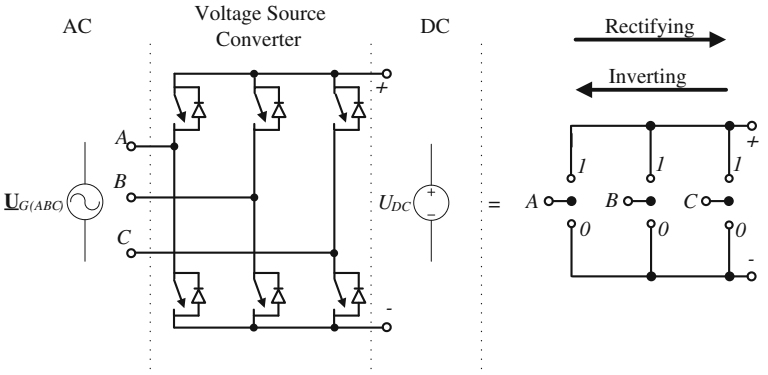

Fig. 5 Voltage Source Converter (VSC) equivalent circuit. Two operating modes are available: rectifying—energy flows from AC to DC circuit and inverting—energy flow direction is from DC to AC circuit

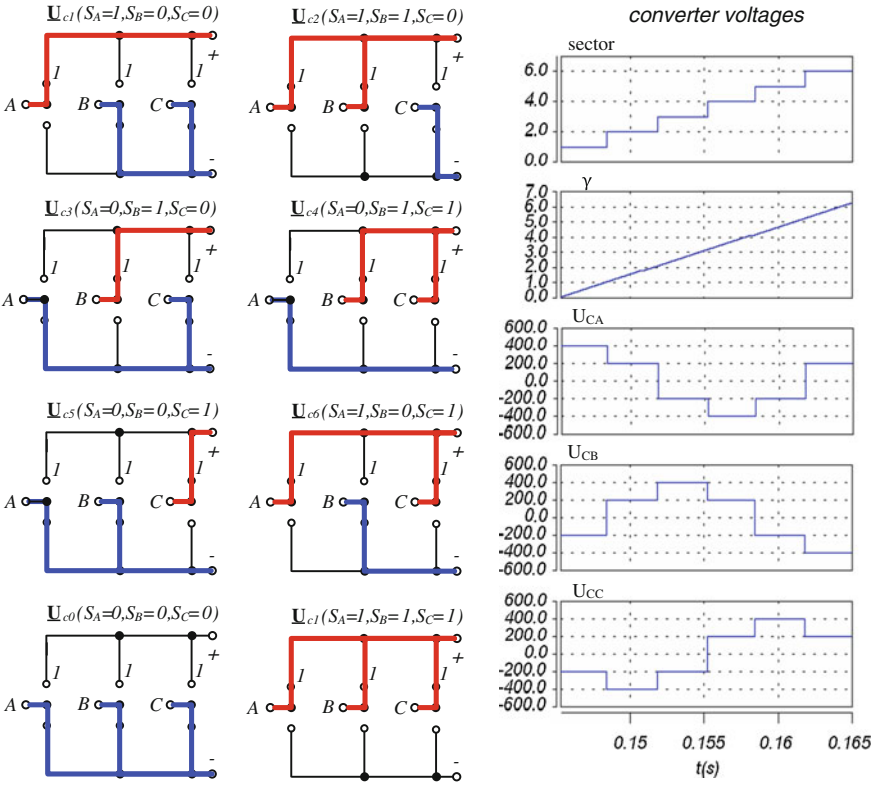

Fig. 6 Three-phase 2-level VSC switching states, modulator signals and phases voltages

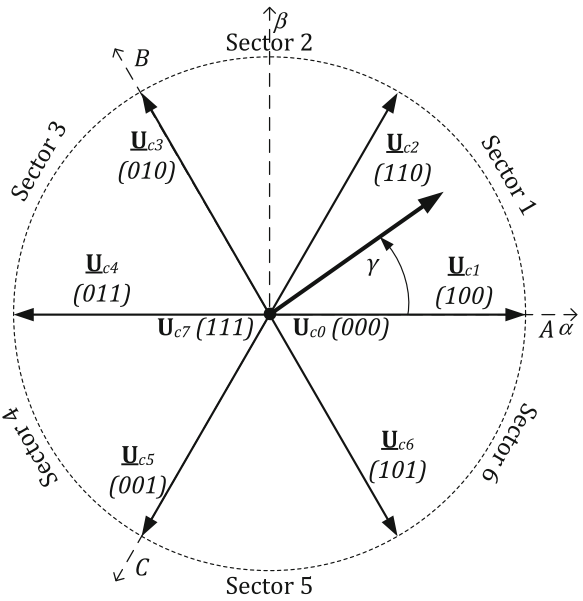

Fig. 7 Voltage source converter AC voltage represented as a SV states

in simpliest solution *L*) and output DC filter C is presented in Fig. 8a, while Fig. 8b shows its single phase representation. Where $\underline{\mathbf{U}}_G$—grid voltage SV, $\underline{\mathbf{I}}_G$—AC current SV, $\underline{\mathbf{U}}_C$—GCC AC terminals voltage SV, and $\underline{\mathbf{U}}_i = \underline{\mathbf{U}}_{LC} + \underline{\mathbf{U}}_{LG}$—a SV of voltage drop on the AC filter (*L* or *LCL*). In case of *LCL* $\underline{\mathbf{U}}_{LC}$—a SV of voltage drop on the converter side inductance L_C, $\underline{\mathbf{U}}_{LG}$—a SV of voltage drop on the grid side inductance L_G, *R*—equivalent resistance of the input filter inductances.

The converter voltage $\underline{\mathbf{U}}_C$ is controllable and depends on switching states and DC voltage level. Through magnitude and phase control of the converter voltage $\underline{\mathbf{U}}_C$, the line current can be controlled by changing the voltage drop on the input filter inductance $\underline{\mathbf{U}}_i$. Therefore, inductances between grid and AC terminals of the GCC are mandatory and important. They create a current source and provide boost feature of the GCC. Through controlling the converter AC voltage $\underline{\mathbf{U}}_C$, the phase and amplitude of the grid current vector $\underline{\mathbf{I}}_G$ is controlled indirectly.

Hence, in Fig. 9 phasor diagrams of GCC are shown in both inverting and rectifying operation. From this figure can be seen that the magnitude of converter voltage $\underline{\mathbf{U}}_C$ is higher during inverting than in rectifying mode. With assumption of a stiff grid (i.e., $\underline{\mathbf{U}}_G$ is an ideal voltage source without internal impedance) terminal voltage of GCC $\underline{\mathbf{U}}_C$ can be higher up to 3 % between rectifying and inverting operation [53, 54].

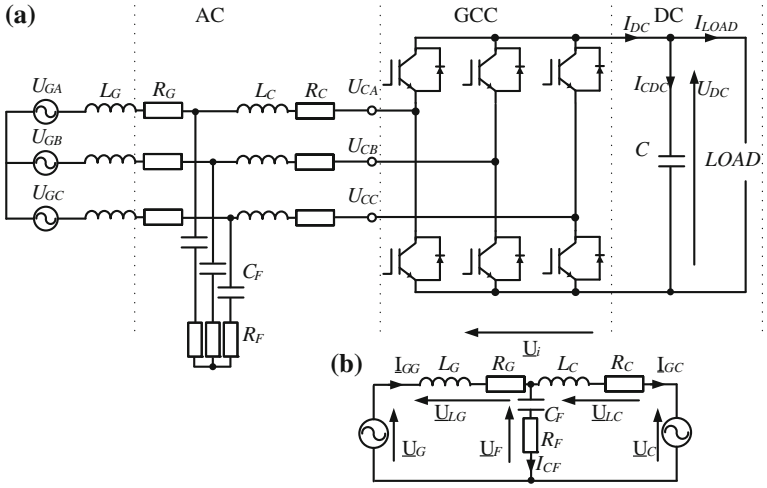

Fig. 8 The GCC: **a** three-phase 2-level circuit, **b** single phase equivalent circuit

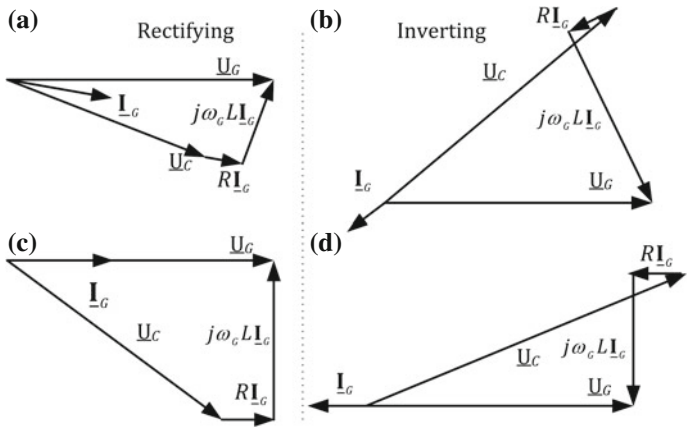

Fig. 9 Phasors diagrams of the GCC: **a**, **b** non-unity power factor in rectifying operation; **c**, **d** unity power factor operation in inverting operation

2.3 Operation Limits of the Grid Converter

From Fig. 9 it can be concluded that for the GCC load current a limit exist with assumption of constant AC grid and DC voltages. The value of AC filter inductance has to be taken into account in this consideration. Below that limit, the GCC is not able to operate and maintain a unity power factor requirement. Low value of the filter inductance and higher voltage reserve (a difference between the AC RMS

voltage and the DC voltage) can increase that limit. The consideration has to be started from the lowest limit of the DC voltage level:

$$U_{DC} > \sqrt{3}\sqrt{2}U_{GRMS} \tag{6}$$

(Example: if $U_{GRMS} = 230V \rightarrow U_{DC} = 2.45 \times 230V = 564V$)

This limitation is introduced by freewheeling diodes in the GCC which operate as an ordinary diode rectifier. This limitation is rather theoretical value. In the literature exists other limitation [45, 48, 53, 54] which takes into account the AC power (value of the AC current) of the GCC.

For simplicity it can be assumed at this stage that $\underline{\mathbf{I}}_G = \underline{\mathbf{I}}_{GG} + \underline{\mathbf{I}}_{GC}$ if $\underline{\mathbf{I}}_{CF} = 0$ for first harmonic of the grid current. Moreover, consider that referenced value of the grid current differ from actual grid current by $\Delta\underline{\mathbf{I}}_G$ and its equals to difference between referenced and actual value of the grid current:

$$\Delta\underline{\mathbf{I}}_G = \underline{\mathbf{I}}_{Gref} - \underline{\mathbf{I}}_G \tag{7}$$

Direction and velocity of the grid current SV changes are described by derivative of that grid current $L{}^{d\underline{\mathbf{I}}_G}/_{dt}$. It can be represented in synchronous dq coordinates as follows:

$$L\frac{d\underline{\mathbf{I}}_G}{dt} + R\left(\underline{\mathbf{I}}_{Gref} - \Delta\underline{\mathbf{I}}_G\right) = \underline{\mathbf{U}}_G - U_{DC}\mathbf{S} + j\omega_G L\left(\underline{\mathbf{I}}_{Gref} - \Delta\underline{\mathbf{I}}_G\right) \tag{8}$$

Assuming resistance of the input inductances $R \cong 0$ and actual grid current is very close to referenced one ($\Delta\underline{\mathbf{I}}_G \approx 0$), Eq. (8) can be rewritten:

$$L\frac{d\underline{\mathbf{I}}_G}{dt} = \underline{\mathbf{U}}_G - U_{DC}\mathbf{S} + j\omega_G L\underline{\mathbf{I}}_{Gref} \tag{9}$$

According to Eq. (9) the direction and velocity of the actual grid current SV changes depends on: L—values of filter inductance, $\underline{\mathbf{U}}_G$—grid voltage SV, $\underline{\mathbf{I}}_{Gref}$—grid current reference SV, U_{DC}—value of the DC voltage level, $\mathbf{S}$—switching signals of the GCC.

Let us consider that six active vectors ($\underline{\mathbf{U}}_{Cref(1\ldots6)}$) of the GCC rotate clockwise in synchronous dq coordinates. For each voltage vector ($\underline{\mathbf{U}}_{Cref(0\ldots7)}$) the current derivatives multiplied by L are denoted as ($P\underline{\mathbf{U}}_{Cref(0\ldots7)}$) [53, 54]. Graphical illustration of Eq. (9) is shown in Fig. 10.

Referenced current $\underline{\mathbf{I}}_{Gref}$ is in phase with line voltage vector $\underline{\mathbf{U}}_G$ and it lies on the axis d. The difference between actual current $\underline{\mathbf{I}}_G$ and referenced $\underline{\mathbf{I}}_{Gref}$ is defined by Eq. (7). Based on the above equations the boundary condition can be given:

$$|U_{DC}\mathbf{S}| = \frac{\sqrt{3}}{2}|\underline{\mathbf{U}}_C| = \left|\underline{\mathbf{U}}_G + j\omega_G L\underline{\mathbf{I}}_{Gref}\right| \tag{10}$$

Assuming that: $\underline{\mathbf{U}}_G = U_{Gmax}$, $\underline{\mathbf{I}}_{Gref} = I_{Gmaxref}$ and $\underline{\mathbf{U}}_C = \frac{2}{3}U_{DC}$ the following expression can be derived:

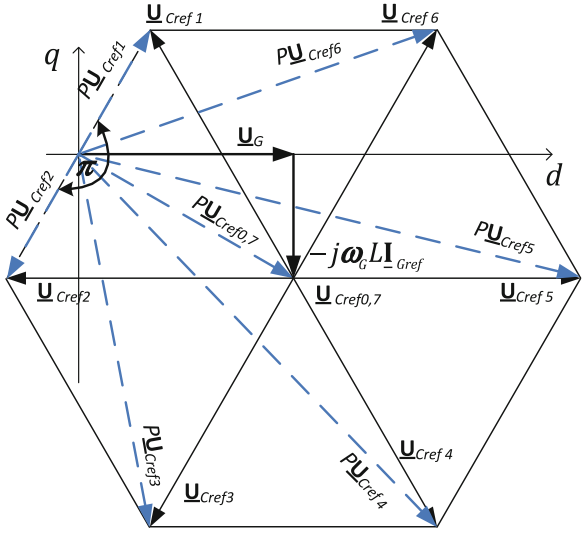

Fig. 10 Graphical illustration of Eq. (9)—instantaneous position of SV and its derivatives [53, 54]

$$\frac{\sqrt{3}}{2}\frac{2}{3}U_{DC} = \sqrt{U_{Gmax}^2 + \left(\omega_G L I_{Gmaxref}\right)^2} \tag{11}$$

Rearranging the equation for minimum DC voltage is obtained:

$$U_{DCmin} = \sqrt{3U_{\mathrm{Gmax}}^2 + 3\left(\omega_G L I_{Gmaxref}\right)^2} \tag{12}$$

Example: $U_{Gmax} = 230\sqrt{2}\,\mathrm{V}, \omega_G = 100\pi\frac{\mathrm{rad}}{\mathrm{s}}, L = 0.01\,\mathrm{H}, I_{Gmaxref} = 10\,\mathrm{A}$;than $U_{DCmin} \geq 566\,\mathrm{V}$

Based on this relation the maximum value of the filter inductance can be derived:

$$L_{max} = \frac{\sqrt{\frac{1}{3}U_{\mathrm{DC}}^2 - U_{\mathrm{Gmax}}^2}}{\omega_G I_{Gmaxref}} \tag{13}$$

Example:

$U_{Gmax} = 325\,\mathrm{V}, \omega_G = 100\pi\frac{\mathrm{rad}}{\mathrm{s}}, I_{Gmaxref} = 10\,\mathrm{A}, U_{DCmin} = 566\,\mathrm{V},$ than $L_{max} = 0.01\,\mathrm{H}$

2.4 Design of LCL Filter

The AC side of grid connected converters has to be installed with *L* or *LCL* filters (Fig. 11). The purpose of the AC filter is to reduce higher harmonics distortion caused by switching process of a power electronics devices. The filtration

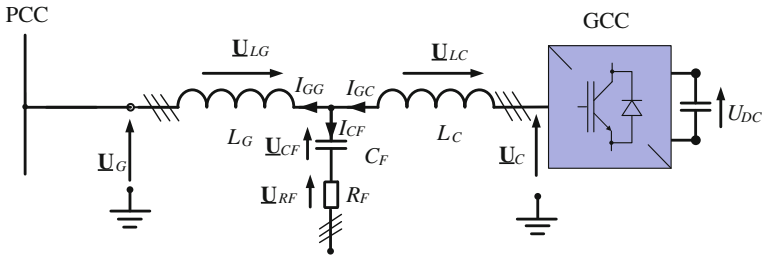

Fig. 11 A *LCL* filter scheme (L_C—converter side inductance, C_F—filter capacitance, R_F—resonance damping resistor, L_G—grid inductance, *PCC*—Point of Common Coupling)

capability of *LCL* filters are significantly higher than simple *L* filter. Therefore, the previous one are more popular in practice. *LCL* filters allows to reduce volume of the filter and assures more effective higher harmonics current filtration in respect to *L* filter. The proper calculation of *LCL* filter parameters are important to obtain stable operation of the GCC. There are several methods to obtain these parameters [46, 55, 56], all of them have to take into account: maximal reduction of higher harmonics caused by switching process with minimum filter volume and reactive power consumption.

For the propose of presented control method the selection of *LCL* filter parameters can be done according to following steps [56]:

1. Define base values

   Base impedance, capacitance and inductance:

$$Z_B = \frac{U_N^2}{P_N}, \quad L_B = \frac{Z_B}{\omega_N}, \quad C_B = \frac{1}{\omega_N Z_B} \tag{14}$$

where $\omega_N = \omega_G = 2\pi 50$—nominal converter pulsation, $U_N = U_{GL-L} = 230\sqrt{3}$—nominal phase to phase converter voltage. Nominal RMS converter phase current can be calculated as:

$$I_N = \frac{P_N}{\sqrt{3}U_N} \tag{15}$$

2. Converter side inductance L_C calculation

   The maximum ripple current $I_{maxripref}$ can be selected between 10 and 25 % of nominal phase current I_N. Let assume that $I_{maxripref} = 0.23$. Than maximum converter side ripple current can be calculated as:

$$I_{maxrip} = \sqrt{2} I_{maxripref} \times I_N \tag{16}$$

According to this the converter side inductance can be derived from:

$$L_C \geq \frac{U_{\mathrm{DC}}}{6 f_{sw} I_{maxrip}} \tag{17}$$

where, f_{sw} is a switching frequency. From the other hand Eq. (13) has to be fulfilled.

3. Filter capacitance C_F calculation

As a next step the AC filter capacitance C_F evaluation is needed. The filter capacitance should be less than 5 % of the base capacitance C_B. Therefore, after assumption that per unit capacitance is 4 % i.e. $C_{Fref} = 0.04 C_B$ the filter capacitance can be derived from:

$$C_F = C_{Fref} C_B = C_{Fref} \frac{1}{\omega_N Z_B} = C_{Fref} \frac{P_{\mathrm{N}}}{\omega_N U_N^2} = 0.04 \frac{P_{\mathrm{N}}}{\omega_N U_N^2} \tag{18}$$

4. Grid side inductance L_G calculation

The grid side AC filter inductance can be derived from:

$$L_G = r_a L_C \tag{19}$$

where, r_a is a ratio between grid and converter side inductances.

The r_a factor can be calculated as:

$$r_a = \left| \frac{1 - HA}{HA\left(1 - L_C C_F \omega_{sw}^2\right)} \right| \tag{20}$$

where, HA is the harmonics attenuation of the phase currents for the switching frequency components $\left(HA = \frac{I_{GC}(h_{sw})}{I_{GG}(h_{sw})}\right)$. In this work $HA = 0.08$ has been chosen.

5. Resonance phenomenon verification

To avoid unexpected and unwonted resonances from grid or converter frequencies active or passive damping should be provided [57, 58]. In case of passive damping a resistance R_F should not be too high because its increase losses of the filter and has strong impact on the efficiency of the GCC. The resonant frequency calculated from:

$$f_{res} = \frac{1}{2\pi} \sqrt{\frac{L_G + L_C}{L_G L_C C_F}} \tag{21}$$

should meets following border conditions:

$$10 f_G \leq f_{res} \leq \frac{f_{sw}}{2} \tag{22}$$

where, f_G is a grid first harmonic frequency i.e. 50 Hz in Europe.

Table 3 Example of *LCL* filter calculation for power series (5–400 kVA), $U_{DC} = 700$ V, $f_{sw} = 5$ kH, $U_{Grms} = 230$ V

P_N (kW)	L_C (mH)	C_F (μF)	L_G (mH)	C (mH)	I_N (A)	I_{DC} (A)
5	9.9	3.98	2.97	0.25	7.22	7.14
15	3.3	11.9	0.99	0.74	21.65	21.43
55	0.9	43.7	0.27	2.73	79.71	78.57
150	0.33	119.4	0.099	7.45	216.5	214.3
250	0.198	199	0.059	12.39	360.8	357.1
400	0.124	318.3	0.037	19.8	577.3	571.4

In Table 3 some *LCL* filter calculation examples for power series (5–400 kVA) are presented. If the control of the GCC has a module of a grid impedance estimator the grid impedance can be taken into account in calculation process, what allows to select filter parameters with higher accuracy [59].

2.5 Choosing of DC Capacitor Parameters

Another step of the GCC design is a DC capacitor parameters selection. The most important parameters of the DC-link capacitor are: rated voltage, leakage current, allowed ripple current and as a results life time. The main factors that have to be taken into account in case of capacitor selection are listed below.

1. DC voltage rated value

The voltage ratio of the DC capacitor is a main parameter that has to be carefully chosen. A stable and predictable DC voltage value should be assured by applied control in the GCC. Relationship between the leakage current and the voltage applied under constant temperature conditions shown in Fig. 12. It can be seen that stability of the DC voltage at desired level is very important for a capacitor life time. In Fig. 12 U_{Ret} (rated voltage) is the DC-link voltage value for which the capacitor has been designed; U_{Su} (surge voltage) is the maximum voltage which can be applied to the capacitor for short periods of time, i.e. up to five times for 1 min per hour.

The standard IEC 60384-4 specifies the above voltages as follows: for $U_{Ret} \leq 315V \rightarrow U_{Su} = 1.15U_{Ret}$ and for $U_{Ret} \geq 315V \rightarrow U_{Su} = 1.1U_{Ret}$ and higher U_F forming voltage. When the DC voltage is equals to forming voltage U_F, the forming process starts. Here large amounts of gas and heat are appear. The DC capacitor is designed to surge voltages U_{Su} for short periods only. High over-anodization (high difference between rated voltage and forming voltage) offers the possibility of producing especially reliable capacitors designed as long-life grade "LL" capacitors in accordance with IEC 60384-1 [60, 61].

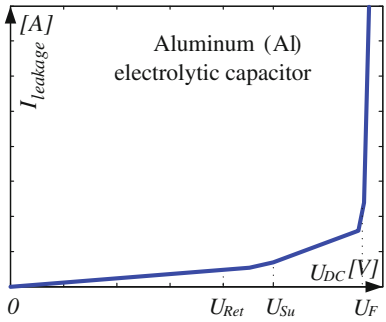

Fig. 12 Current-voltage characteristic of an aluminum (Al) electrolytic capacitor [60, 61]

2. Consideration of ripple current

The term ripple current is used for the RMS value of the AC current that flows through the device as a result of any pulsating or ripple voltage. In Fig. 13 ripple current waveforms for different cases in DC of the GCC connected with AL by DC-link (AC-DC-AC converter) are shown: (a) classical old-fashion AC-DC-AC converter with diode rectifier, (b) AC-DC-AC converter with GCC without information about power consumed by AL (without Active Power Feed-Forward (APFF) which will be discussed further in this chapter), (c) AC-DC-AC converter with GCC with energy flow dynamic improvement between GCC and AL (with APFF).

The maximal permissible ripple in DC current value depends on the ambient temperature, the surface area of the capacitor (i.e. heat dissipation area), the dissipation factor (or Equivalent Series Resistance (ESR)) and on the AC frequency.

Thermal stress has a strong impact on the capacitor's life. Therefore, the dissipation heat generated by the ripple current is an important factor affecting the useful life. Thermal considerations imply that, under certain circumstances, it may be necessary to select a capacitor with a higher voltage or capacitance rating then would be required. The ripple current is a function of the switching frequency. The term useful life or—service life, operational life, or life time is defined as the life achieved by the capacitor without exceeding a specified failure rate. This time can be extended by operating the capacitor at loads below the rating value, lower voltage, current, or temperature and by appropriate cooling system [48, 60].

The ripple in the DC voltage is a function of the ripple current in the DC-link. The capacitor current I_{CDC} is difference between the current I_{DC} (DC current of the GCC) and I_{LOAD} (DC current of a load) as shown in Eq. (23).

A minimum occurs when the DC currents I_{DC} and I_{LOAD} pulses from the both converters overlap (Fig. 14b, c). It can occurs when the pulses are centered on the same time instant. To obtain this conditions a modulation with symmetric zero vector placement can be implemented [62, 63]. PWM pulses are always centered on the half period of the switching state. Fig. 14 shows simulated DC voltage and DC currents I_{DC}, I_{LOAD}, and capacitors current I_{CDC}, I_{CLOAD} over sampling period. It should be noticed that there are a lot of modulation techniques and the problem of modulation and its impact on the controlled system performance (switching

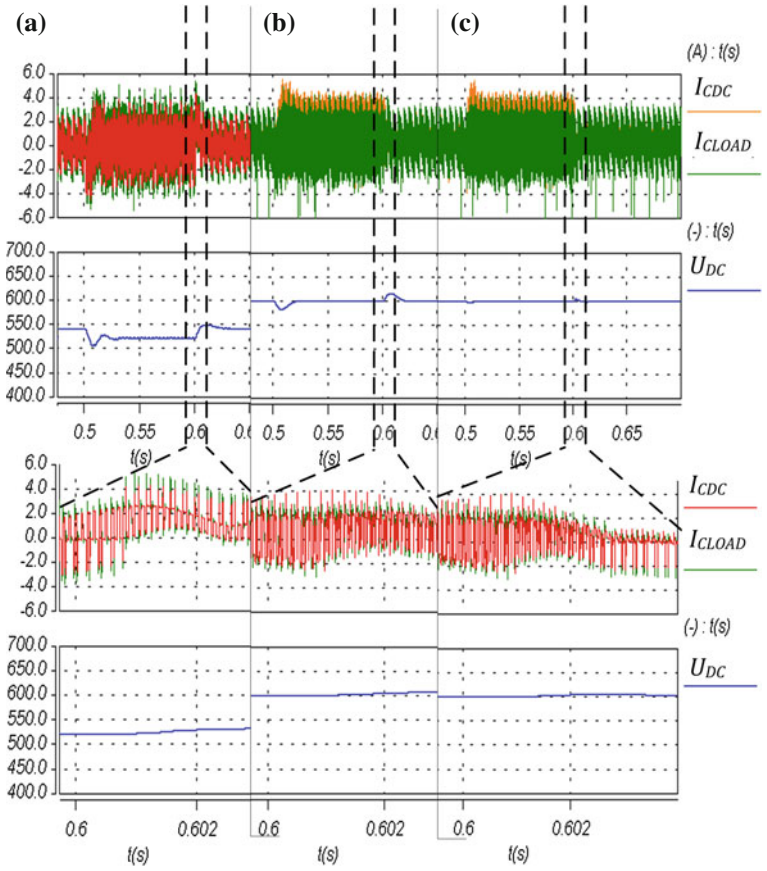

Fig. 13 Ripple current in DC-link capacitors. **a** Classical AC-DC-AC converter with diode rectifier, **b** AC-DC-AC converter with GCC without information about energy flow at AL converter side (without APFF), **c** AC-DC-AC converter with GCC, with information about energy flow at AL side in active power control loop (with APFF). DC-link capacitor C = 470 μF, S_n = 5 kVA. From the *top* capacitor currents, DC voltages and zoom of them

losses, current or voltage shapes, and noise level etc.) are presented in many valuable publications [62–71] and will not be discussed in this chapter.

Summarizing when DC capacitor is under selection all mentioned points has to be determine: the DC voltage rated value, switching frequencies (both AC-DC converters in AC-DC-AC back-to-back converter), topology of an AC-DC converter, and if appropriate, dynamics and accuracy of applied control methods [48, 72]. In novel, environment friendly solution a diode rectifier in AC-DC-AC converters should be avoided because of: single direction energy flow, higher DC voltage fluctuation and ripples (Fig. 13). Therefore, in this chapter only GCC will be described. Its controllability provides more degree of freedom in DC voltage regulation process. The control dynamic and accuracy is higher than in the case of a

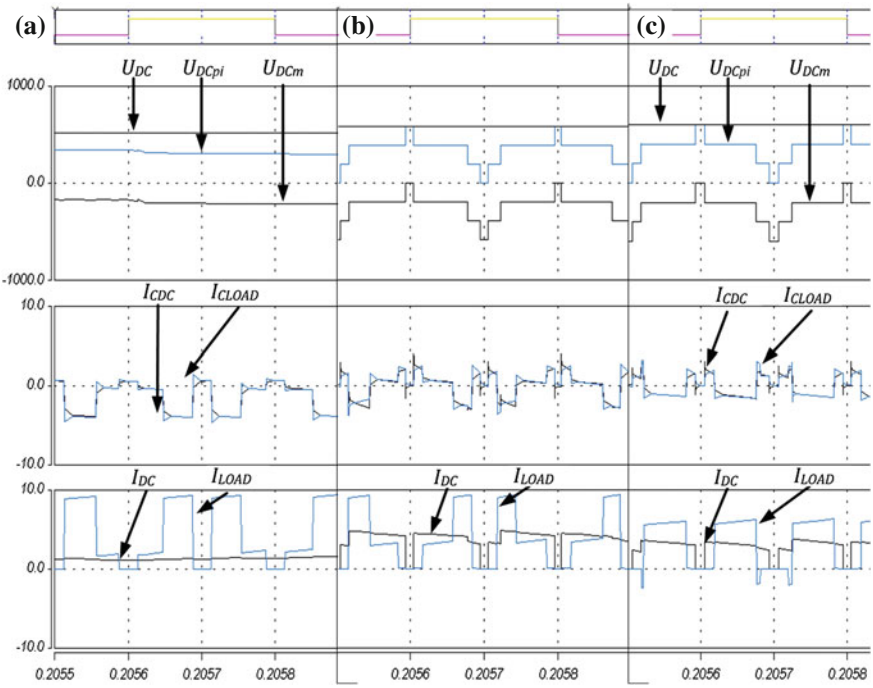

Fig. 14 Simulated ripple in DC currents. **a** Classical AC-DC-AC converter with diode rectifier, **b** AC-DC-AC converter with GCC without information about energy flow at AL converter side (without APFF), **c** AC-DC-AC converter with GCC, with information about energy flow at AL converter side (with APFF); C = 470 μF, S_n = 5 kVA. From the *top* period of sampling, DC voltage and its potentials (positive and negative), capacitors current, DC currents I_{DC}, I_{LOAD}

diode grid side rectifier as shown in Fig. 13b, c. Please take a look also at the waveforms in Fig. 14 over one sampling period during operation just after load step (from 0 to 85 %). It can clearly be seen that the highest current flows from the DC capacitor in the case presented in Fig. 14a. The average value is negative. It means the energy is transferred from the capacitor to the load. In Fig. 14b the capacitor current is significantly reduced. Finally further reduction of the current I_{CDC} is observed in Fig. 14c, here information about the energy at a load side is taken into account in control of the GCC (see APFF description further in this chapter).

3. Calculation of DC capacitance value

Beside variety design criteria [72–74] of the DC-link capacitor, the minimum capacitance value is designed to limit the DC ripple voltage at a specified level, typically ΔU_{DCrip} is 1 or 2 % of U_{DC}. Therefore, peak-to-peak ripple voltage in DC-link is adopted as the design criterion for the DC capacitance determination.

With assumption of a balanced tree-phase grid and neglecting the power losses in the power switches, the GCC's DC part can be derived:

$$C\frac{dU_{DC}}{dt} = I_{DC} - I_{LOAD} \approx \sum_{k=A}^{C} I_{Lk}S_k - \frac{P_{LOAD}}{U_{DC}} \tag{23}$$

For given allowable peak ripple voltage and switching frequency, the minimum capacitor for the GCC converter can be calculated as [26]:

$$C_{min1GC} = P_{maxLOAD}\frac{\sqrt{2} + \frac{\sqrt{3}U_{L-L}}{U_{DC}}}{2\sqrt{3}\Delta U_{DCrip}f_{sw}U_{L-L}} \tag{24}$$

where U_{L-L} is a line-to-line voltage, $P_{maxLOAD}$—maximal load power, ΔU_{DCrip}—specified peak-to-peak ripple voltage in DC voltage under steady states operation. This capacitance can be calculated based on different equations. An alternative approach of the DC capacitance determination, takes into account energy exchange between capacitance and load:

$$\Delta W_{DC} = T_{UT}\Delta P_{maxLOAD} \tag{25}$$

where T_{UT} is a sum of small time constant. From this equation the maximum DC voltage fluctuation under maximal load power step is proportional to energy variation:

$$\Delta U_{\mathrm{maxDC}} = \frac{\Delta W_{DC}}{U_{DC}C_{min2GC}} \tag{26}$$

where ΔU_{maxDC} denotes maximum DC voltage fluctuation under maximal load step, C_{min2GC}—minimal DC capacitance. Transforming Eq. (25), the capacitance can be calculated [48]:

$$C_{min2GC} = \frac{T_{UT}\Delta P_{maxLOAD}}{U_{\mathrm{DC}}\Delta U_{maxDC}} \tag{27}$$

Please take into your consideration that C_{min1GC} capacitance value is lower than C_{min2GC}. The one among other reason is that in T_{UT} time constant not only sampling (equals to switching frequency) is taken into account but also DC voltage filter measurement time delay. It depends on developer which formula will be taken within the process of capacitor sizing. For more details see also [48, 72].

2.6 Modeling of a Grid Connected Converter

There are several publication about modeling of the GCC mentioned above. However, for a reader convenience one of them in stationary $\alpha\beta$ coordinates is presented below. It is useful for description of a vector control method further in this chapter. So, the GCC can be presented as:

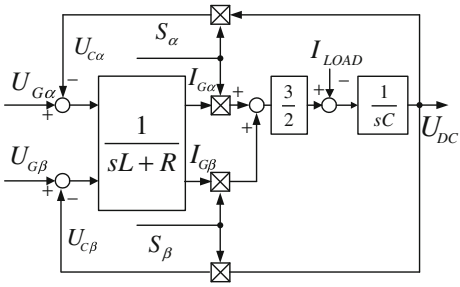

Fig. 15 Model of a three-phase GCC in stationary $\alpha\beta$ coordinates

AC side related with AC filter:

$$L\frac{d\underline{\mathbf{I}}_G}{dt} + R\underline{\mathbf{I}}_G = \underline{\mathbf{U}}_G - U_{DC}\mathbf{S} \tag{28}$$

and, DC side related with DC filter:

$$C\frac{dU_{DC}}{dt} = \frac{3}{2}Re[\underline{\mathbf{I}}_G\mathbf{S}^*] - I_{LOAD} \tag{29}$$

After decomposition into α and β components:

$$L\frac{dI_{G\alpha}}{dt} + RI_{G\alpha} = I_{G\alpha} - U_{DC}S_\alpha \tag{30}$$

$$L\frac{dI_{G\beta}}{dt} + RI_{G\beta} = I_{G\beta} - U_{DC}S_\beta \tag{31}$$

$$C\frac{dU_{DC}}{dt} = \frac{3}{2}\left(I_{G\alpha}S_\alpha + I_{G\beta}S_\beta\right) - I_{LOAD} \tag{32}$$

where,

$$S_\alpha = \left\{S_A - \frac{1}{3}(S_A + S_B + S_C)\right\}, S_\beta = \frac{1}{\sqrt{3}}(S_B - S_C). \tag{33}$$

The graphical representation of Eqs. (30)–(33) are presented in Fig. 15.

The model in Fig. 15 is simple and give a sufficient basic for further consideration. Presented in this chapter RDPC-SVM control method of the GCC uses this model for calculations of system variables in algorithm.

2.7 Selected Control Methods for Grid Converter

Under control methods authors mean a way of currents regulation based on sensor or sensor-less operation of the considered GCC system.

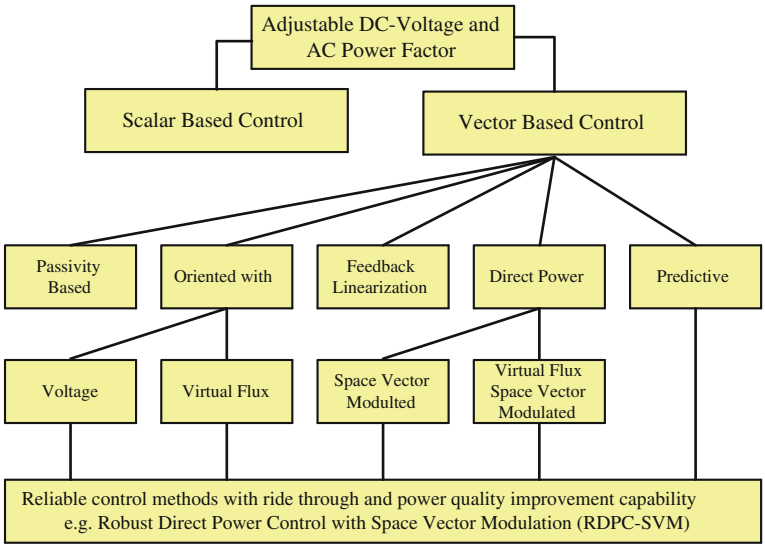

Fig. 16 Classification of a GCC control methods

With above knowledge the control methods can be classified as is presented in Fig. 16. The simplest scalar control method is based on current regulation in three-phase system (AC waveforms) [75, 76]. However, the unceasing development in the DSP platforms give better possibilities for implementation of more and more demanding control methods like model predictive control [77, 78], or additional sophisticated control modules devote to ride-through different problems in power system i.e. voltage distortion e.g. dips, and higher harmonics etc. [51, 52, 79–89].

Similar to ASD, the vector control of the GCC is a general control philosophy that can be implemented in many different ways. The most popular method, known as *Voltage Oriented Control* (VOC) [21, 45, 57, 58, 79, 80] gives high dynamic and static performances via internal current control loops. In the VOC the GCC equations are transformed from stationary to rotating synchronously with the grid voltage coordinates. To improve the robustness of VOC scheme a *Virtual Flux* (VF) concept was introduced by Duarte, Malinowski [45]. However, from the theoretical point of view, other types of mathematical coordinates transformations can be defined to achieve decoupling and linearization of the GCC equations. This has originated the methods known as nonlinear control. Jung and Lee proposed a nonlinear transformation of GCC state variables so that, in the new coordinates, the DC voltage and grid current are decoupled by feedback; this method is called also *Feedback Linearization Control* (FLC). Moreover, a *Passivity Based Control* (PBC), was also investigated in respect to the GCC [90–94].

In the 1990s have been expanded the idea of *Direct Torque Control* (DTC) for the GCC called *Direct Power Control* (DPC) [95–98]. From that time it has been continuously improved [45, 93]. However, these control principles are very similar to DTC schemes and have the same drawbacks. Therefore, to overcome that

disadvantages a *Space Vector Modulator* (SVM) [99] was introduced into DPC structure giving new DPC-SVM control scheme [100]. In recent years a novel *Predictive Control* (PrC) methods has been also implemented in GCC. Moreover, to increase reliability (ride-through) of control and finally total immunity of power electronics equipment in case of power systems disturbances a special function for classical, basic control methods can be implemented [51, 85].

2.8 Basic Control Methods

Many interesting control methods are proposed in the literature (see above). However, in this chapter we will focus on DPC-SVM investigated by research group of Kazmierkowski [32]. In this method instead of hysteresis controllers the classical PI controllers was used and the switching table was replaced by SVM. This improvement assures constant switching frequency and join the advantage of VOC (modulator i.e. low switching frequency is needed) and DPC (active and reactive power closed control loops) in one control scheme. Hence, it is quite comfortable for DSP implementation (for industry) [101]. The DPC-SVM has a simple structure, low number of coordinates transformation and assure good steady states and dynamic properties. The block diagram is presented in Fig. 17. It has to be stressed that in case of distorted grid voltage the DPC-SVM with Phase Lock Loop (PLL) cannot guarantee sinusoidal shape and balanced AC grid phase currents.

The DPC-SVM control algorithm consist of: active and reactive instantaneous power estimator, two inner powers control loops and one outer DC voltage control loop. Estimated powers are compared with referenced values, the differences (errors) are delivered to the PI controllers. Reference value of the reactive power is set by user, while reference value of the active power is calculated based on measured DC voltage of the converter and its reference value set by user. Output signals from powers PI controllers determine GCC referenced voltage in dq coordinates. After transformation to stationary $\alpha\beta$ coordinates signals are given to SVM input. The output SVM signals determinates current states of the transistors. There is a possibility to control both active and reactive powers independently (reactive power compensation realized by the GCC). In fact there are a little coupling between each other however it can be omitted in further consideration [48]. Reactive power can vary according to grid demand for reactive power while active power is varying according to DC voltage output PI controller signal. The instantaneous power estimator can be constructed in stationary $\alpha\beta$ coordinates as follows:

$$P = \left(U_{G\alpha} I_{G\alpha} + U_{G\beta} I_{G\beta}\right) \tag{34}$$

$$Q = \left(U_{G\alpha} I_{G\beta} - U_{G\beta} I_{G\alpha}\right) \tag{35}$$

where $U_{G\alpha}, U_{G\beta}, I_{G\alpha}, I_{G\beta}$ are components of the grid voltage and the grid current in stationary $\alpha\beta$ coordinates.

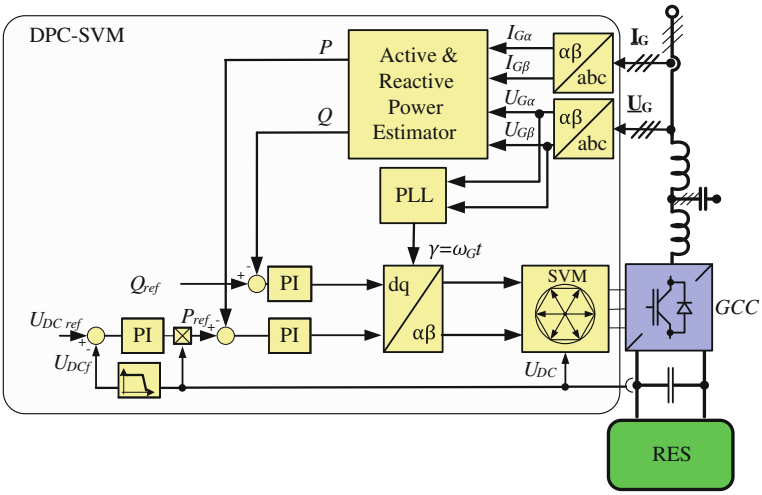

Fig. 17 Block scheme of Direct Power Control with Space Vector Modulation (DPC-SVM) and Phase Lock Loop (PLL)

Fig. 18 Phase Lock Loop (PLL) block scheme

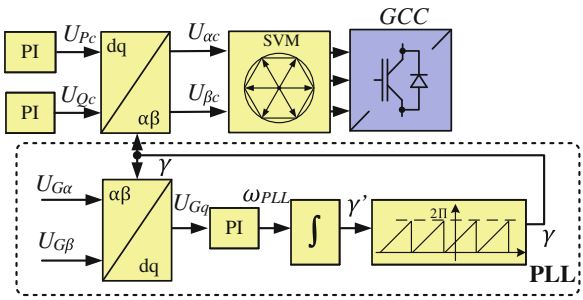

Important part of the control method is a PLL block (Fig. 18). In the PLL measured grid voltage components in stationary $\alpha\beta$ coordinates are transformed to synchronously rotating dq coordinates. Then, PI controller is minimizing of the q axis component which is responsible for the grid voltage SV angle. This angle is used for coordinates transformation in DPC-SVM control structure.

2.9 Voltage Dips Compensation Module

Hereafter, it is assumed that reader knows the GCC converter with basic control structure like DPC-SVM. Now, it is possible to implement a special functionalities

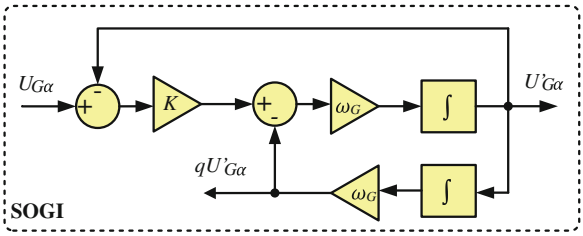

Fig. 19 Block scheme of a Second Order Generalized Integrator (SOGI) [85]

realized by additional control modules dedicated specially for standards and requirements needs. This sophisticated functions can be longer and more complicated than main algorithm itself. But let us focus only on selected, mature methods. The function should be simple in implementation and work in any operation conditions [85].

Voltage dips can appear in power systems quite often because e.g. of short circuits or intentionally on/off process of heavy loads. Usually sudden voltage changes can disturb operation of a power electronics converters control. In this case a converter can produce unsymmetrical and non-sinusoidal current. Moreover, in a DC voltage significant 100 Hz fluctuation can appears.

Additional control module designed for dips compensation provides symmetrical currents processed by the GCC in each phases for any kind of dips. The dips compensation module split unsymmetrical voltage into positive and negative sequence voltage components. In this case the negative voltage component is a main source of information about appearing voltage distortion. Separated voltage components can be used in DPC-SVM control structure with following rules and modifications:

- Implementation of the additional module of the AC voltage components extraction.
- New power estimator based on positive voltage components and actual AC grid current.
- DC voltage band-stop filter (notch filter) to eliminate fluctuation caused by negative voltage component.
- Grid voltage negative component feed-forward to referenced the SVM's input signals.

According to a definition, each asymmetry in three phase system can be represented by sum of a voltage components: positive, negative and zero sequence signals. By analogy it is possible to describe the three-phase system in stationary $\alpha\beta$ coordinates by two components: positive (rotating with grid frequency) and negative (rotating with grid frequency but in opposite direction), e.g. (36):

$$\underline{\mathbf{U}}_G = \underline{\mathbf{U}}_{Gp} e^{j\omega t} + \underline{\mathbf{U}}_{Gn} e^{-j\omega t} \tag{36}$$

where $\underline{\mathbf{U}}_{Gp}, \underline{\mathbf{U}}_{Gn}$—complex value of positive and negative voltage components respectively.

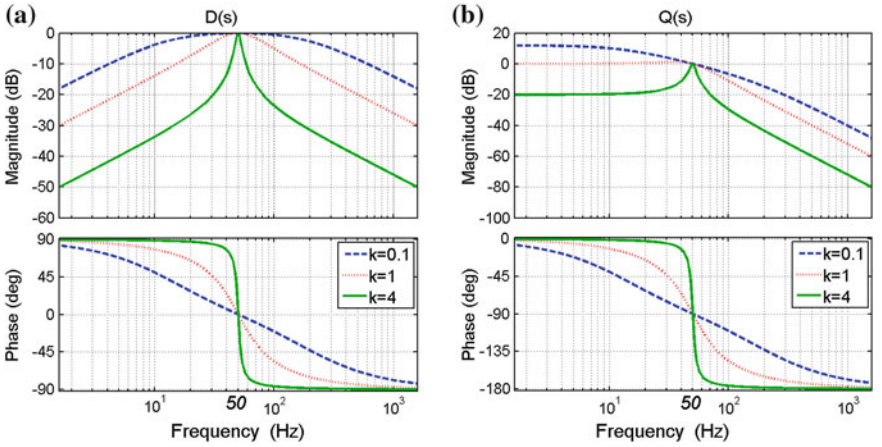

Fig. 20 Bode diagram for transmittances: **a** $D(s)$, **b** $Q(s)$

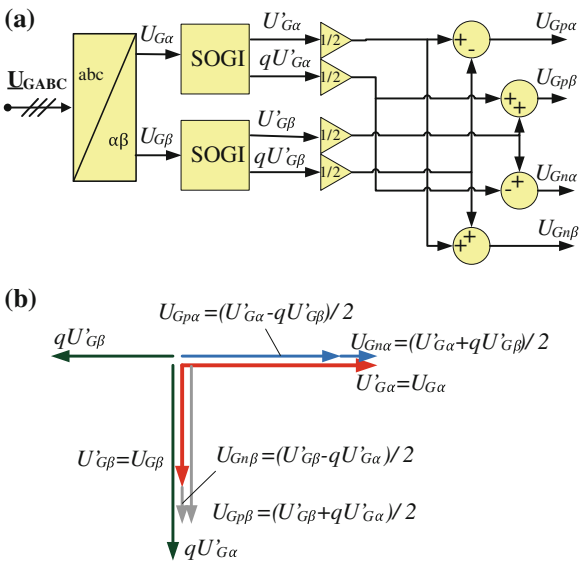

Fig. 21 Positive and negative components extraction from $U_{G\alpha}, U_{G\beta}$ actual grid voltage in the stationary $\alpha\beta$ coordinates: **a** block scheme for negative and positive voltage components separation, **b** vector diagram of the component separation process

The extraction and separation process of these components is realized by Second Order Generalized Integrator (SOGI) [85]. The SOGI block scheme is presented in Fig. 19. The SOGI transmittances $D(s)$ and $Q(s)$ are described by Eqs. (37) and (38):

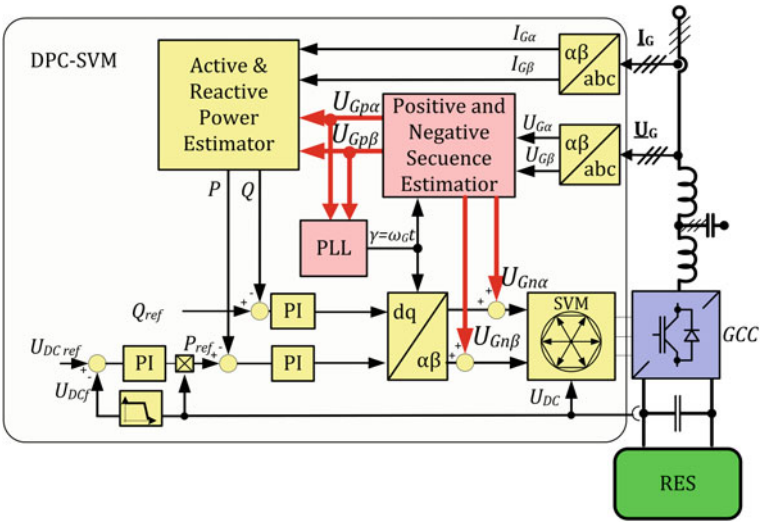

Fig. 22 Voltage Dips Compensator (VDC) module implemented in basic DPC-SVM vector control method

$$D(s) = \frac{U'_{G\alpha}}{U_{G\alpha}}(s) = \frac{k\omega_G s}{s^2 + k\omega_G s + \omega_G^2} \tag{37}$$

$$Q(s) = \frac{qU'_{G\alpha}}{U_{G\alpha}}(s) = \frac{k\omega_G^2}{s^2 + k\omega_G s + \omega_G^2} \tag{38}$$

The frequency characteristic of the SOGI are show in Fig. 20. As can be seen the $D(s)$ transmittance operates as a low-pass filter, while $Q(s)$ transmittance provides a 90° phase shift for filtered $U'_{G\alpha}$ signal.

Hence, output signals of the SOGI are: filtered input signal of grid voltage component and its 90° shifted equivalent. Using the SOGI for both $U_{G\alpha}, U_{G\beta}$ components in $\alpha\beta$ coordinates system it is possible to extract positive and negative components of these voltages. The graphical representation of this solution is presented in Fig. 21.

Such Voltage Dips Compensator (VDC) module can be implemented in the basic vector control structure as presented in Fig. 22.

2.10 Higher Harmonics Compensation Module

Increasing number of nonlinear loads connected to the power system induce several problems mainly related with higher harmonics distortion. Undesired harmonics cause higher losses and devastation of electrical equipment connected

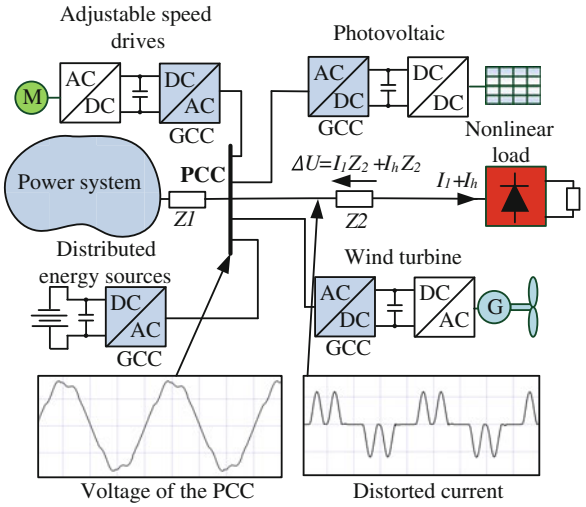

Fig. 23 Simplified section of a power system with a set of various devices and high power nonlinear load

to the power system. Moreover, higher harmonics can destroy power system devices e.g. transformers. Higher harmonics issues are related with both, voltage and current. Nonlinear loads (e.g. diode rectifiers) introduce to the grid hardly distorted current which can causes grid voltage distortion related to transmission line and grid impedances. All loads which are not properly secured and prepared for operation under distorted voltage conditions can work faultily or be damaged amplifying the distortion. Figure 23 presents sample power system operating with distorted voltage. The GCC which is the scope of this chapter operates as an interface between the grid and distributed active load (e.g. renewable energy sources, adjustable speed drives, and electric vehicles etc.). The modern power electronic converter should work correctly with distorted line voltage, not causing amplification of distortion, not disturbing operation of other devices and if it is possible be able to compensate harmonic distortion by rectifying/inverting sinusoidal current from/to the grid. To achieve this functionalities it is necessary to extend control algorithm by additional harmonics compensation control module described below.

Presented harmonics compensation algorithm operates based on extraction of higher harmonics from measured grid current. The extracted signal is gained and finally added to referenced voltage at the input of the SVM. Block scheme of control algorithm with additional function—current Higher Harmonic Compensation (HHC) module is presented in Fig. 24.

Grid voltage distorted by higher harmonics can be described as follows:

$$\underline{\mathbf{U}}_G = U_1 e^{j\gamma} + U_5 e^{-j5\gamma} + U_7 e^{j7\gamma} + \cdots + U_{(6k\mp1)} e^{\mp j(6k\mp1)\gamma} \tag{39}$$

where, $\gamma = \omega_G t$; k = 1, 2, …

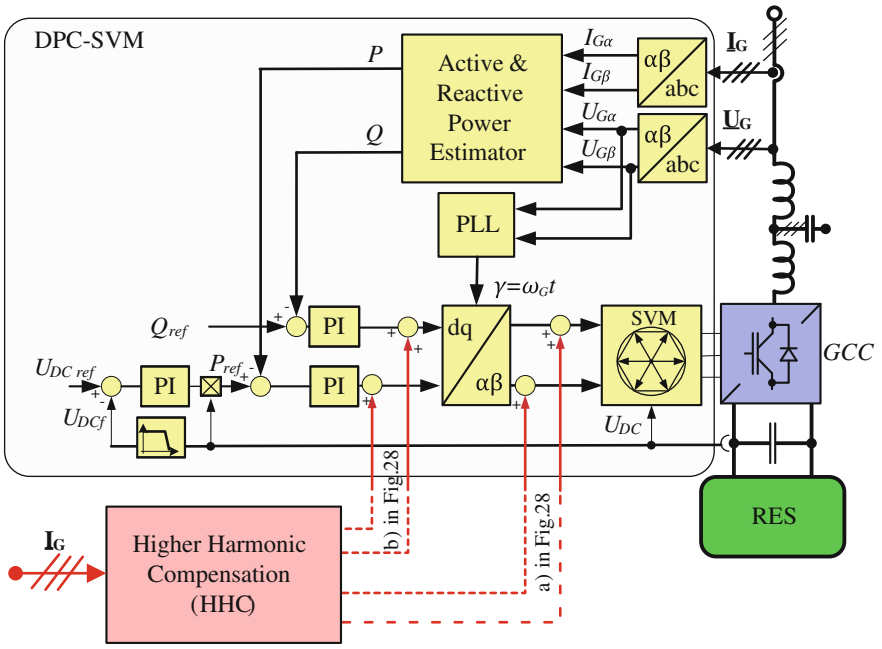

Fig. 24 Block scheme of the control method with Higher Harmonic currents Compensation (HHC) module

The most significant and frequently occur harmonics in the grid are: 250, 350, 550 and 650 Hz. There is simple relation between harmonics order and their rotating direction:

- positive harmonics, rotating in the same direction as fundamental one and can be expressed as: 3k + 1 (1, 4, 7, 10…),
- negative harmonics, rotating in the opposite direction to the fundamental and can be expressed as: 3k + 2 (2, 5, 8, 11…),
- zero harmonics, with no phase shift between themselves can be expressed as: 3k + 3 (3, 6, 9, 12…).

The idea of harmonics description rotating in positive and negative direction can be seen in the SV diagram (Fig. 25a) or harmonics spectrum in different coordinates (Fig. 25b) (stationary $\alpha\beta$ coordinates and dq coordinates rotating synchronously with grid voltage fundamental component vector (i.e. with frequency 50 or 60 Hz)).

Higher harmonics extraction from measured signal can be realized by the GCC control as follows:

- In synchronous coordinates—measured values of the currents are transformed into rotating coordinates system dq [82]. As a reference signal (angle) multiplication of the fundamental harmonic phase angle is used. Respectively for 5th

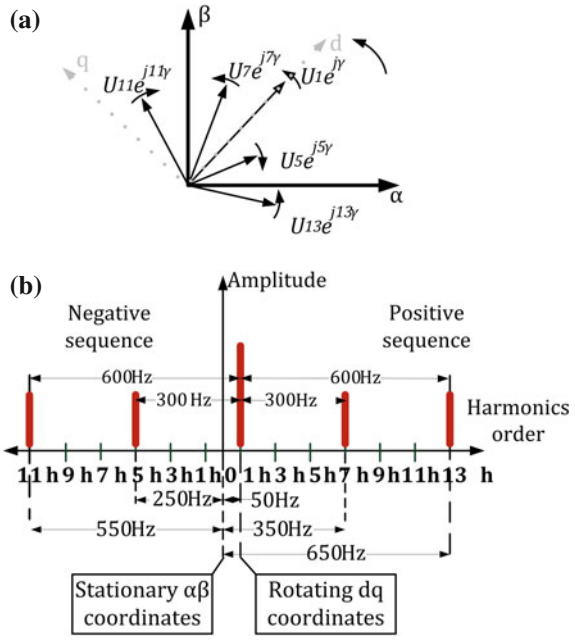

Fig. 25 Illustration of positive and negative sequence harmonics components based on 5th, 7th, 11th and 13th harmonics: **a** space vector diagram in stationary $\alpha\beta$ coordinates, **b** harmonics spectrum

harmonic multiplication by 5 of the fundamental phase angle, 7th is multiplication by seven, etc. After transformation each harmonics are represented by DC components. It gives possibility for extraction constant signal (voltage) which level gives information about each harmonics contend in measured current. To avoid distortion and oscillations in measured signal proper filters should be used. Compensation signal with opposite sign and tuned gain is given as an additional element (HHC block) to the reference values for the SVM.

- Filtration in stationary $\alpha\beta$ coordinates with a Resonant Controllers (RC). The RCs are used as a high-band tuned band-pass filters applied in closed control loops [83]. Transfer function of an ideal band-pass filter is as follows:

$$U_h(s) = K_i \frac{s}{s^2 + (h\omega)^2} \tag{40}$$

where K_i is a gain of the filter, ω is a resonant frequency and h is an order of the harmonics.

Bode diagram of an ideal resonant filter expressed by Eq. (40) for different gain values (Ki) are presented in Fig. 26a.

The resonant frequency is set to 250 Hz. For ideal band-pass filter the gain is infinity. Because of very narrow pass-band the frequency characteristic of the filter has to be exactly matched to frequency of the compensated harmonics. Any difference between measured and assumed frequency can cause improper operation and even lost stability of the control algorithm. To avoid this disadvantage

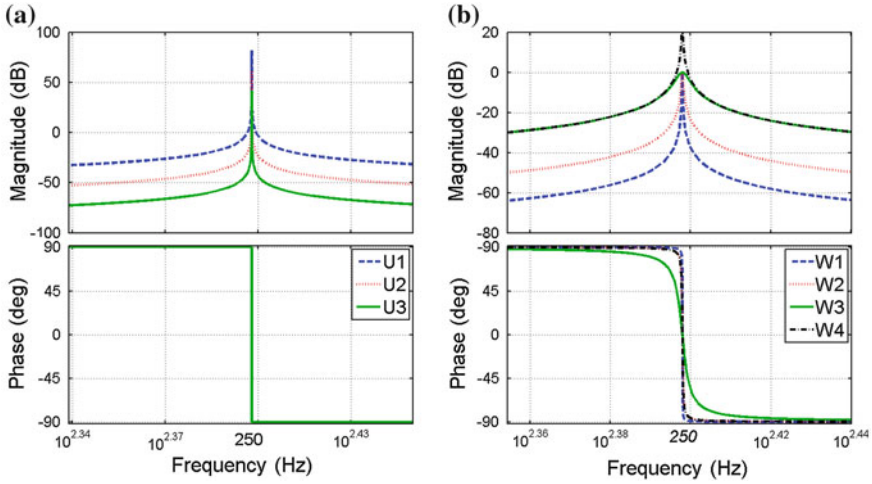

Fig. 26 Bode diagram of the resonant controllers tuned to 250 Hz frequency: **a** ideal RC with different filter gains: $K_{i(U1)} = 0.01$, $K_{i(U2)} = 1$, $K_{i(U3)} = 100$; **b** non-ideal RC with different filter gains (Ki) and pass-band width (ω_c): K_i ($K_{i(W1)} = K_{i(W2)} = K_{i(W3)} = 1$, $K_{i(W4)} = 10$) and ω_c ($\omega_{c(W1)} = 0.1$, $\omega_{c(W2)} = 1$, $\omega_{c(W3)} = 10$, $\omega_{c(W4)} = 1$)

structure of non-ideal band-pass filter should be used. The transfer function of non-ideal resonant band-pass filter is as follows:

$$W_{hN}(s) = K_i \frac{\omega_c s}{s^2 + \omega_c s + (h\omega)^2} \tag{41}$$

where K_i is a gain of the controller, ω_c defines width of the pass-band and slope steepness of the filter, h is an order of the harmonic.

Bode diagram of the non-ideal resonant filter for different gain values (Ki) are shown in Fig. 26b.

It can be observed that extending the pass-band results in reduction of the filter slope steepness what gives worse selectivity of the filter. It is the reason why the balance between filter accuracy and width of the pass-band need to be kept.

To separate particular harmonics in stationary $\alpha\beta$ coordinates system a single filter tuned for each frequency is required. But taking into consideration fact that rotating directions are easy to observe and harmonics are symmetrical in terms of rotating coordinates dq it is possible to extract two harmonics using only one RC, what is shown in Fig. 25b. It can be noticed that for control algorithm both 5th and 7th harmonics are observed as 300 Hz frequency harmonic.

Block diagrams of both presented harmonics compensation methods are presented in Fig. 27.

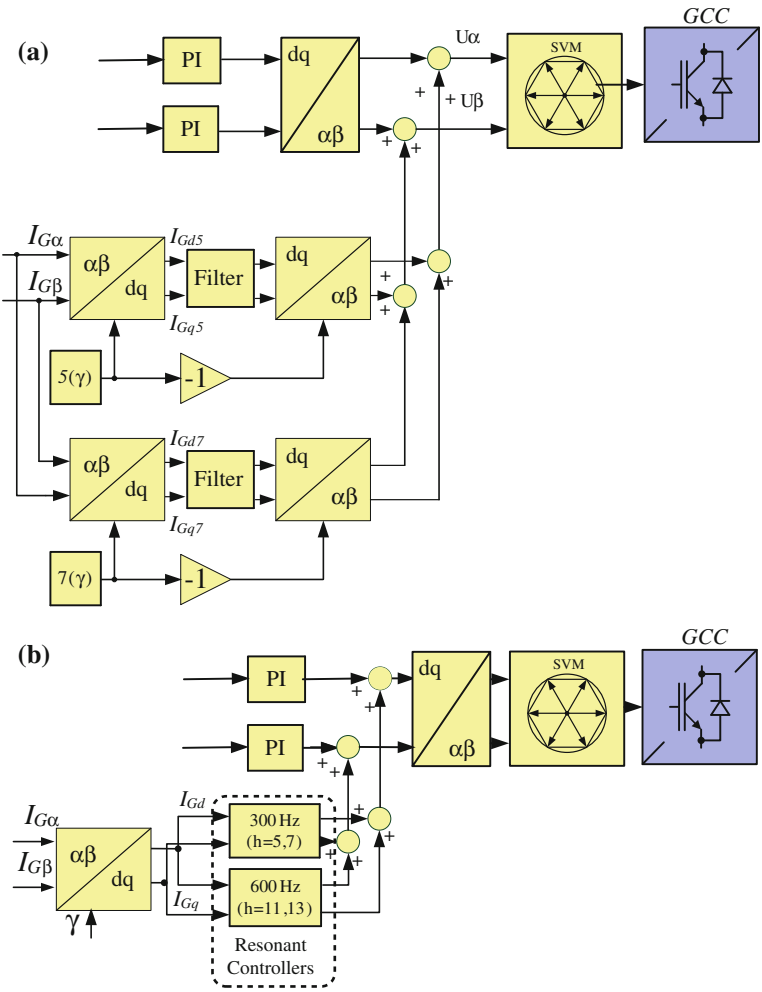

Fig. 27 Block diagram of Higher Harmonic Compensation (HHC) module realized by using: **a** Synchronous Coordinates, **b** Resonant Controllers (RES)

2.11 Active Power Feed-Forward (APFF) Module

The GCC connected to the power system should operates as an universal interface between the grid and different electrical devices (Fig. 23), providing high dynamics and stability of the control algorithm independently from the type of connected device. To achieve this functionality another control module: Active Power Feed-Forward (APFF) is introduced.

The APFF which gives information about the active power flow between the GCC and the grid can be applied as an additional module to the main control

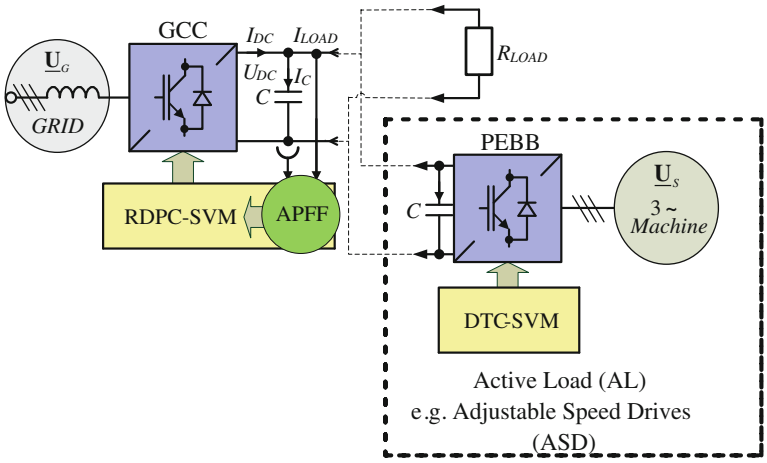

Fig. 28 Block diagram of the GCC system with the Active Power Feed-Forward (APFF) control module based on instantaneous values of DC voltage and current

algorithm of the GCC. To get an information about instantaneous value of the active power exchanged between the converter system and the grid, without need of implementation additional current and voltage sensors following method is proposed. Estimated active power is product of instantaneous DC voltage and current, as is shown in Eq. (42).

$$P_{GC} = U_{DC} \times I_{DC} \tag{42}$$

Block diagram of the GCC system with additional Active Power Feed-Forward control module is presented in Fig. 28

To achieve stable operation of the control algorithm with the APFF control module some additional filters on the measured DC current are needed. Figure 29 shows selected voltages and currents waveforms in the grid converter system interconnecting AL (e.g. consisted of an ASD) within transient responds to step changes of the machine load torque without (Fig. 29a) and with APFF (Fig. 29b) control module. It can be observed that implementation of the proposed APFF allows for significant reduction of the DC voltage fluctuations during load transients.

2.12 Impact of Grid Impedance

In this subsection impact of an increased grid impedance on a GCC with LCL filter is presented. Figure 30 shows block scheme of the considered system with additional high value of the grid impedance L_{GS}.

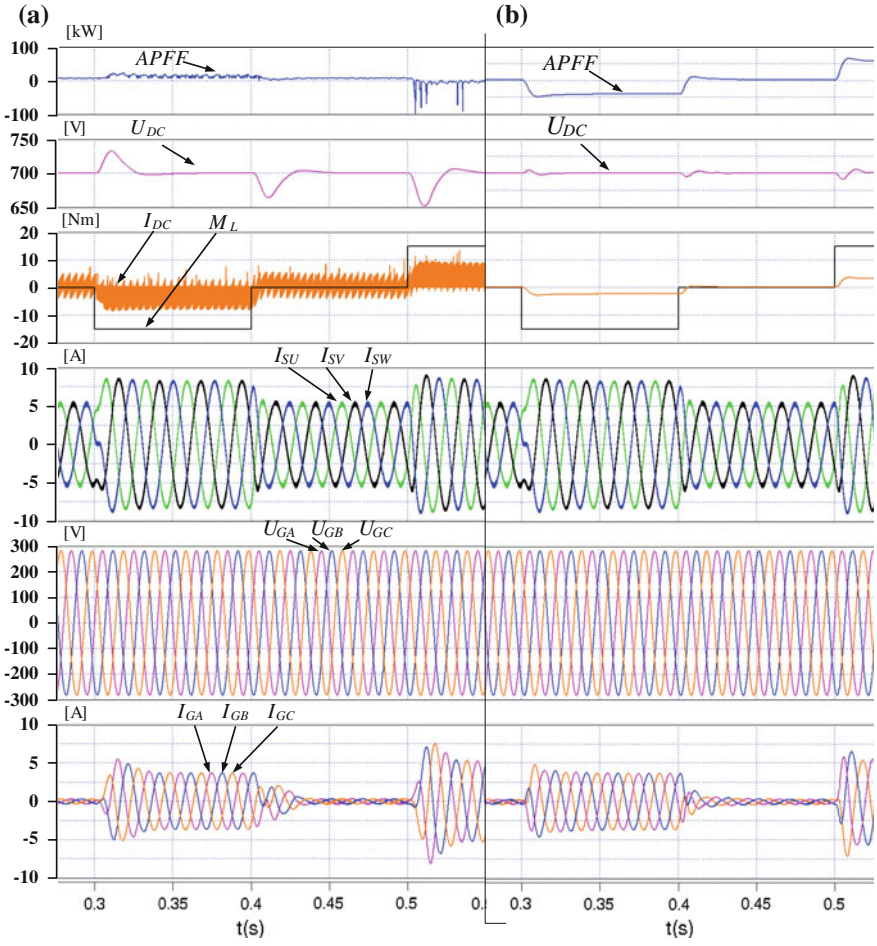

Fig. 29 Influence of Active Power Feed-Forward (APFF) applied in the GCC system interconnecting AL (e.g. ASD). System operates: **a** without APFF; **b** with APFF. From the *top* *APFF*—estimated active power (kW); U_{DC}—DC voltage (V); I_{DC}—DC current (A); M_L—machine load torque (Nm); I_{S1}, I_{S2}, I_{S3}—machine stator currents (A); U_{GA}, U_{GB} U_{GC}—grid voltage (V); I_{GA}, I_{GB}, I_{GC}—grid currents (A)

2.13 Rectifying Operation of the Grid Connected Converter

Behavior of the system during rectifying operation of the GCC has been verified. A borderline values of the grid impedance for rectifying operation of the GCC have been found for different nominal powers of the system and collected in Table 4. Figure 31 presents voltages and currents of the system while the grid

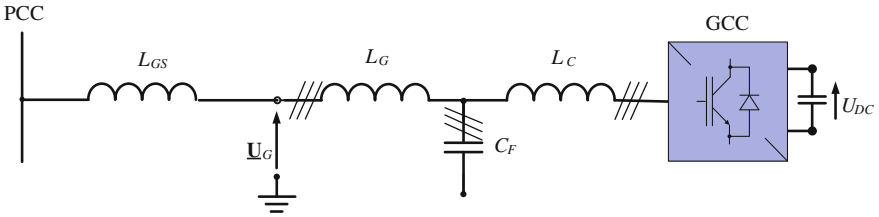

Fig. 30 Block diagram of GCC and LCL filter system with additional high grid impedance L_{GS}

Table 4 Parameters of the LCL filter for selected power ranges of the system during rectifier operation with DC load (*DC LOAD*)

GCC rated power (kW)	L_C (mH)	C_F (μF)	L_G (mH)	L_{MGS} (mH)	*DC LOAD* (Ω)
5	9.9	3.98	2.97	60	147
15	3.3	11.9	0.99	20	49
55	0.9	43.7	0.27	4	13.36
400	0.124	318.3	0.037	0.125	1.84

Estimated borderline values of grid impedance for stable operation of the system (L_{MGS})

impedance (L_{GS}) is increasing. As it can be seen above the maximal value of the grid impedance (L_{MGS}) system loses its control stability.

2.14 Inverting Operation of the Grid Connected Converter

Behavior of the system during inverting operation of the GCC has been also tested. A borderline values of grid impedance under inverting operation have been found for selected power ranges of the system and collected in Table 5. In Fig. 32 voltages and currents of GCC system are presented while grid impedance (L_{GS}) is increasing. As it can be notice again after exceed maximum value of the grid impedance (L_{MGS}) system lose stability. Obtained value of the grid impedance is higher than in case of rectifying operation. Moreover it should be noticed that DC voltage is suddenly increasing while in case of rectifying operation the DC voltage is decreasing or is more unstable (Fig. 31d).

Based on presented simulation and experimental study following conclusion can be formulated: before connecting GCC to the electrical network to provide efficient and stable operation of the system a grid impedance should be known. It can be estimated by GCC itself by use of additional grid impedance estimation module. For further information please refer to [51, 52, 59, 87].

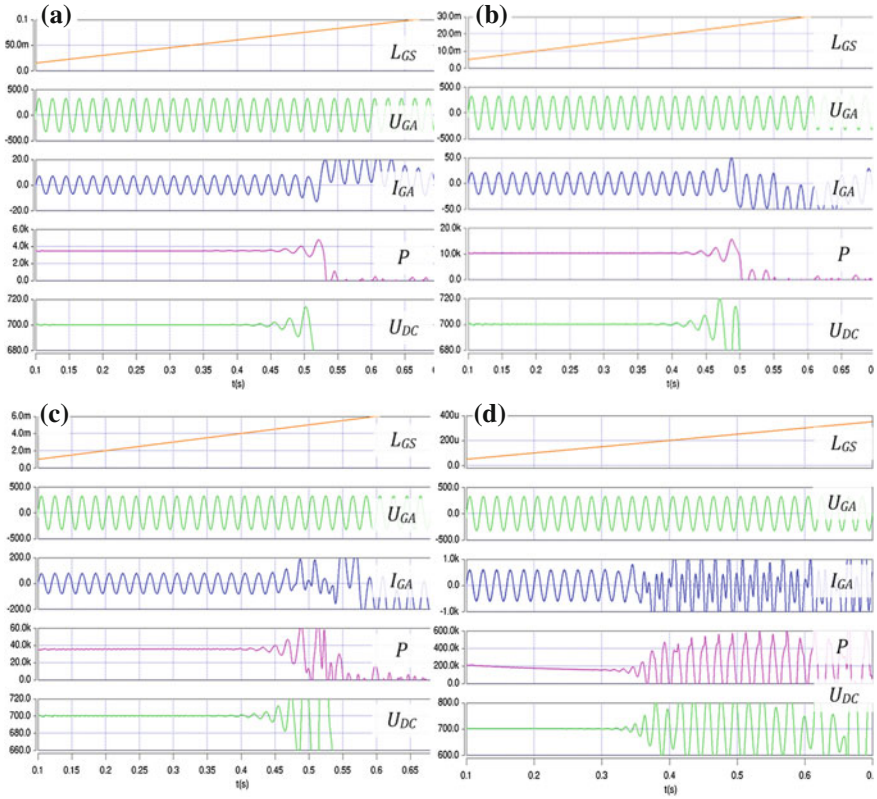

Fig. 31 Grid voltage and current waveforms during rectifying operation of the GCC with increasing grid impedance (L_{GS}). For different nominal power values of the GCC: **a** 5 kW; **b** 15 kW; **c** 55 kW; **d** 400 kW. From the *top* grid impedance (mH, μH), U_{GA} grid voltage in phase A (V), I_{GA} grid current in phase A (A), P estimated active power (kW), U_{DC} DC voltage of the GCC (V)

Table 5 Parameters of the LCL filter for selected power ranges of the system during inverting operation with DC current source I_{DC}

GCC rated power (kW)	L_C (mH)	C_F (μF)	L_G (mH)	L_{MGS} (mH)	I_{DC} (A)
5	9.9	3.98	2.97	70	5.3
15	3.3	11.9	0.99	22	15
55	0.9	43.7	0.27	5.5	70
400	0.124	318.3	0.037	0.3	550

Estimated borderline values of grid impedance for stable operation of the system L_{MGS}

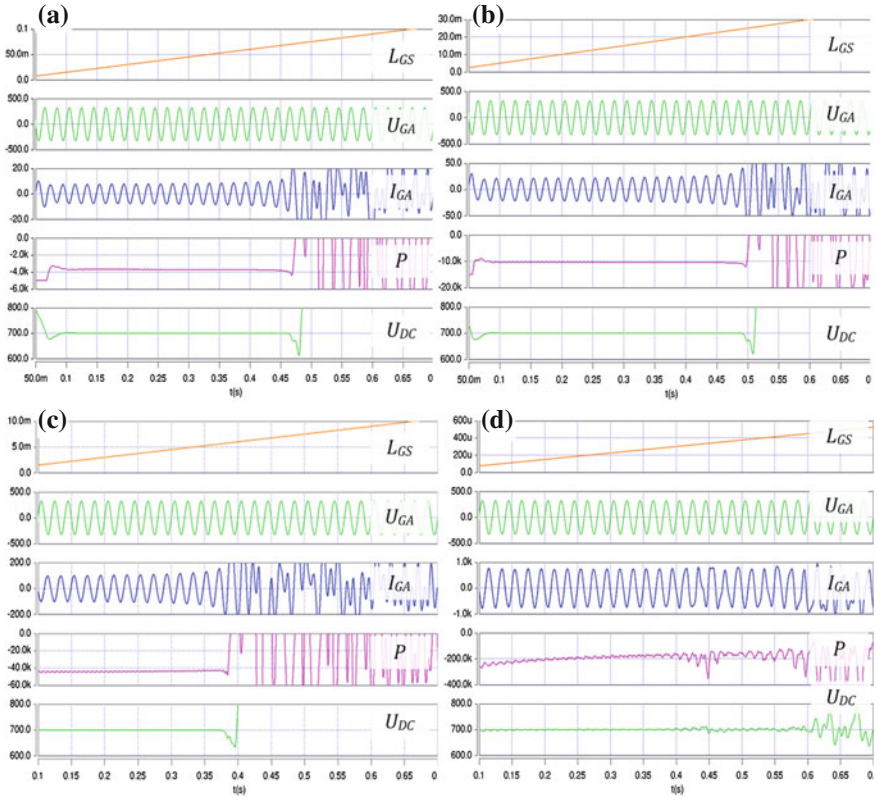

Fig. 32 Grid voltage and current waveforms during rectifier operation of the GCC with increasing grid impedance (*LGS*). For different nominal power values of the GCC: **a** 5 kW, **b** 15 kW, **c** 55 kW, **d** 400 kW. From the *top LGS* grid impedance (mH, μH), *UGA* grid voltage in one phase (V), converter current in one phase (A), estimated active power (kW), DC voltage of the GCC (V)

2.15 Reliable Control Method to Grid Voltage Disturbances

As it has been mentioned all presented control modules can be integrated in final control method of the GCC operating in distributed energy system. Thanks to additional modules developed control method is reliable in respect to grid voltage dips and higher harmonics. Hereafter, this new control algorithm can be presented as Robust Direct Power Control with Space Vector Modulation (RDPC-SVM). The term "*robust*" in the name of proposed control refers to the fact that the RDPC-SVM method is expected to operate in an uncertain environment with respect to the system dynamic. In the literature it can be found that:

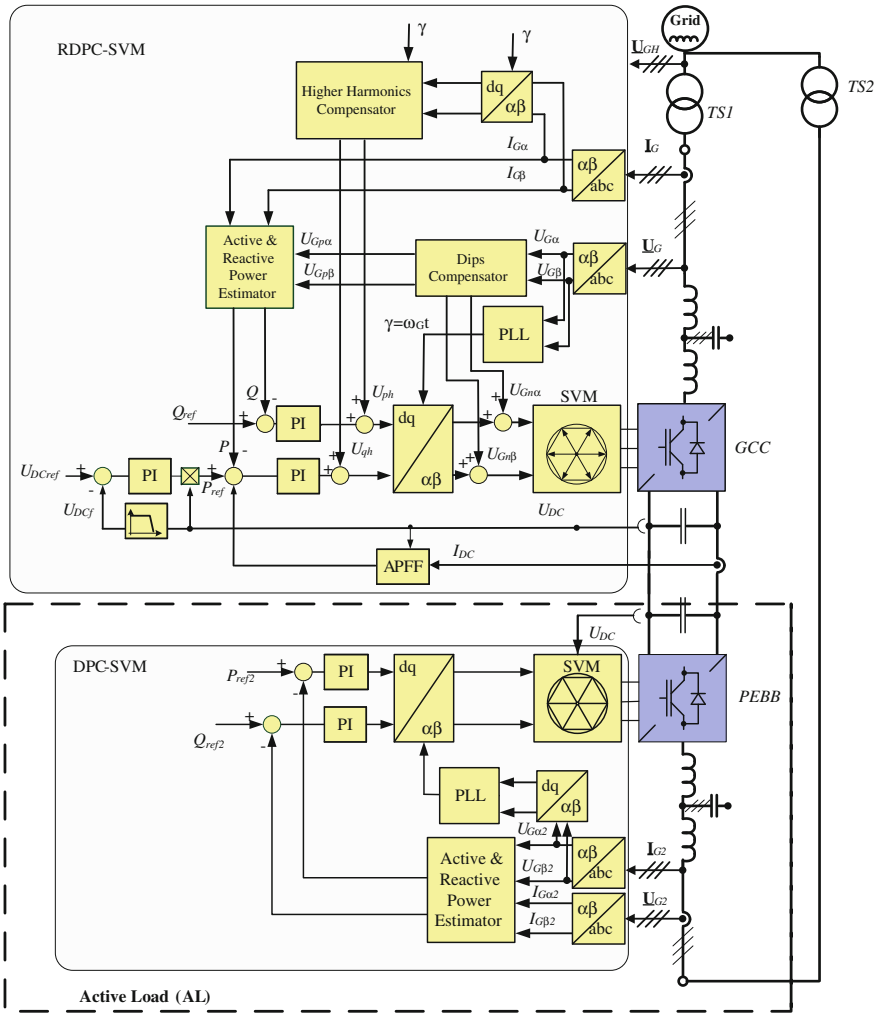

Fig. 33 Block diagram of developed Robust Direct Power Control Space with Space Vector Modulation (RDPC-SVM) applied for control the GCC in an AC-DC-AC system interconnecting energy sources

There are several ways in which systems can be uncertain, and in this course we will target the main three: (1) The initial conditions of a system may not be accurately specified or completely known; (2) Systems experience disturbances from their environment, and system commands are typically not known a priori. *(3) Uncertainty in the accuracy of a system model itself is a central source. Any dynamical model of a system will neglect some physical phenomena, and this means that any analytical control approach based solely on this model will neglect some regimes of operation* [102].

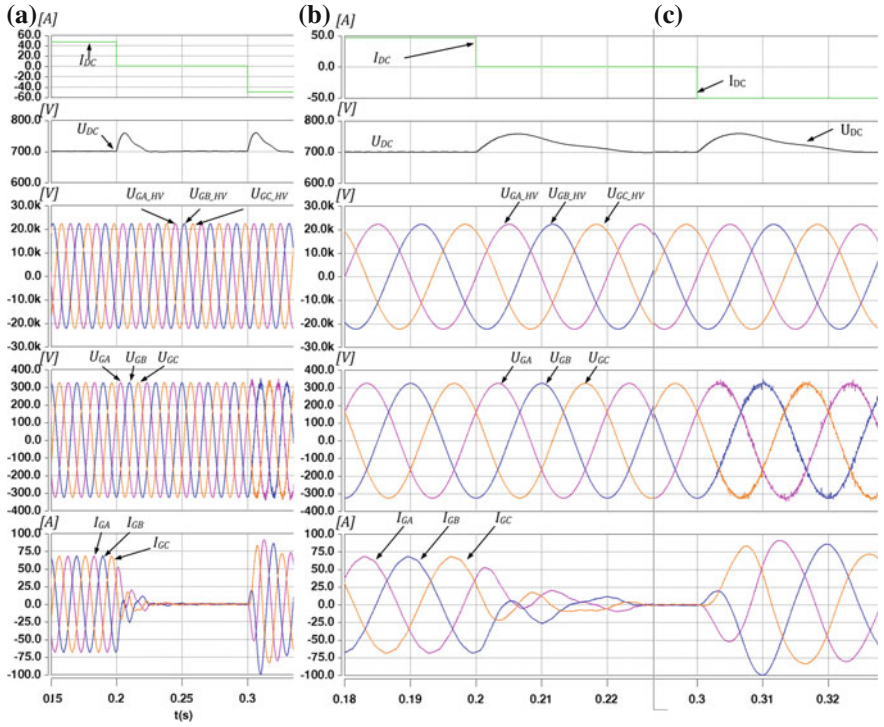

Fig. 34 Operation of the 55 kW the GCC with the RDPC-SVM under different operation modes. The GCC operation mode change: **a** from rectifying to no-load operation and to inverting mode; **b** zoomed step change from rectifying to no-load operation; **c** zoomed step change from no-load to inverting operation. From the *top* I_{DC}—DC-link current (A); U_{DC}—DC-link voltage (V); U_{GA_HV}, U_{GB_HV}, U_{GC_HV}—voltage on the high side of the grid transformer (V); U_{GA}, U_{GB}, U_{GC}—voltage on the low side of the transformer (V); I_{GA}, I_{GB}, I_{GC}—phase grid currents (A)

In our case all three mentioned points can be somehow found in the real power system and the GCC operation. Therefore, the reliable RDPC-SVM control algorithm is consisted of following control modules:

- Direct Power Control with Space Vector Modulation (DPC-SVM) for control converter currents and DC voltage of the GCC, with Active and Reactive Power Estimators.
- Grid angle synchronization using Phase Locked Loop (PLL) for grid angle estimation.
- Voltage Dips Compensation (VDC).

– Voltage positive and negative component extraction using Dual Second Order Generalize Integrator (DSOGI). Negative Component Voltage Feed-Forward.
– 100 Hz DC voltage notch filter.

- Active Power Feed-Forward control using active power estimation based on instantaneous values of DC voltage and current.
- Higher Harmonic Compensation (HHC) (based on Resonant Controllers).

The block diagram of the presented RDPC-SVM control method applied to the GCC in an AC-DC-AC interconnecting energy sources is shown in Fig. 33. Further, some selected simulation results showing operation of the RDPC-SVM control algorithm are presented. To achieve operation conditions like in a typical power system the model of 3-phase 15 kV/400 V grid transformer has been used with parameters based on producers datasheet [103].

As it can be seen in Fig. 34 the GCC operates properly during different operation modes. Applied additional control modules have no negative impact on dynamic of the control system.

Figure 35 presents operation of the GCC with RDPC-SVM scheme supplied by distorted grid voltage (high order harmonics and voltage dips). It can be observed that due to additional control modules the grid currents are controlled to be sinusoidal like and symmetrical in spite of grid voltage disturbances. Good results are obtained in steady and in transient states.

Finally Fig. 36 shows operation of the GCC with RDPC-SVM supplied by significantly distorted voltage (high order harmonics and voltage dips).

3 Experimental Test Bench

In this subsection the behavior of discussed system and control method is presented under experimental conditions, similar to these which can appear in the real power system. To verify proper operation of described control method an experimental test bench has been developed for selected power of the GCC (3, 5, 15, 55 kW). Laboratory setup is composed of the GCC (scope of interest) and another DC-AC (treat as a PEBB). To reflect operation in real power system following configuration of the test bench has been proposed:

- The AC-DC-AC system interconecting two different AC voltage sources—scheme of the system is presented in Fig. 37. This configuration allows to model connection of two different power systems (e.g. with different frequencies or voltage levels) with bidirectional energy flow. The GCC has been controlled by RDPC-SVM control algorithm.
- The AC-DC-AC system operates in closed loop of power circuit—scheme of the system is presented in Fig. 38. This system configuration allows for bidirectional power flow as well as arranging different operating conditions for the GCC with AL. It gives also ability for operation of both converters under nominal power while from the grid only energy covering the system losses are used. As in previous case in the grid side converter the RDPC-SVM control method has been implemented and verified by series of experimental tests.

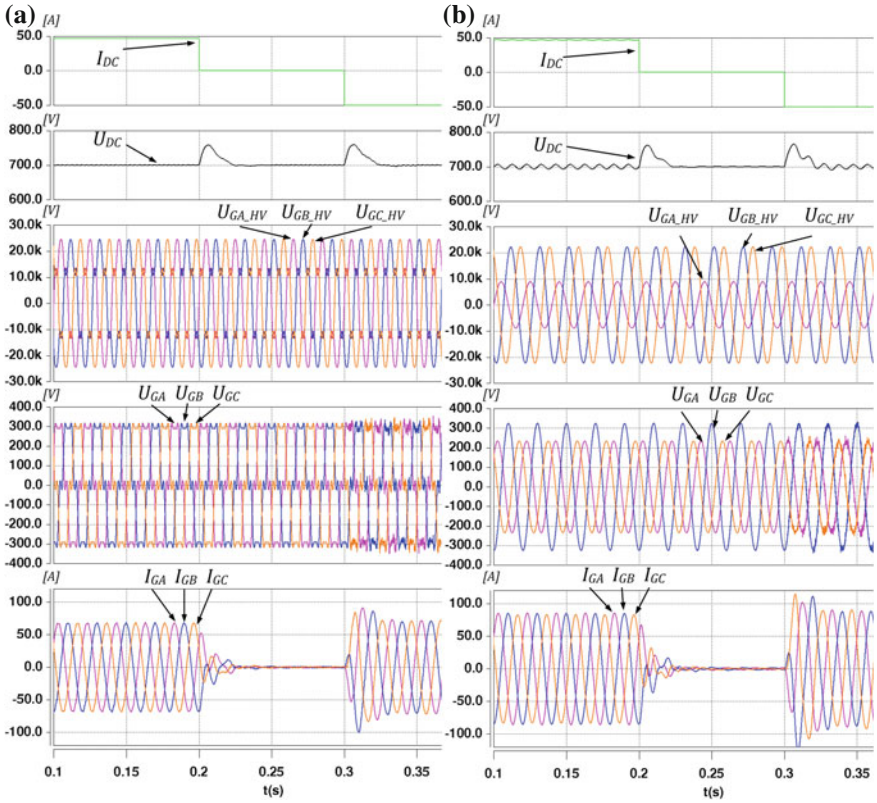

Fig. 35 Operation of 55 kW the GCC with the RDPC-SVM during transients with grid voltage disturbances. The GCC operation mode step change: **a** from rectifying, to no-load operation and to inverting operation, grid voltage distorted by high order harmonics (20 % of 5th and 10 % of 7th harmonics); **b** from rectifying to no-load operation and to inverting operation, grid voltage distorted by 60 % dip in phase A. From the *top* I_{DC}—DC-link current (A); U_{DC}—DC-link voltage (V); U_{GA_HV}, U_{GB_HV}, U_{GC_HV}—voltage on the high side of the grid transformer (V); U_{GA}, U_{GB}, U_{GC}—voltage on the low side of the transformer (V); I_{GA}, I_{GB}, I_{GC}—phase grid currents (A)

Figure 39 shows voltages and currents of the GCC with implemented basic DPC-SVM algorithm. The converter is working under distorted grid voltage (30 % voltage dip in one phase) condition. As it can be noticed: without dips compensation module the converter currents are unbalanced and non-sinusoidal. The current the THD factor is around 20 %.

Similar situation is shown in Fig. 40 (50 % voltage dip in one phase) but with proposed the RDPC-SVM control algorithm. It can be seen that converter currents are kept sinusoidal and symmetrical. In spite of high grid voltage disturbances, the current the THD factor is below 1.0 %. This feature of the GCC significantly reduce the negative impact of power electronics converter on the grid voltage, especially under distorted voltage and high grid impedance.

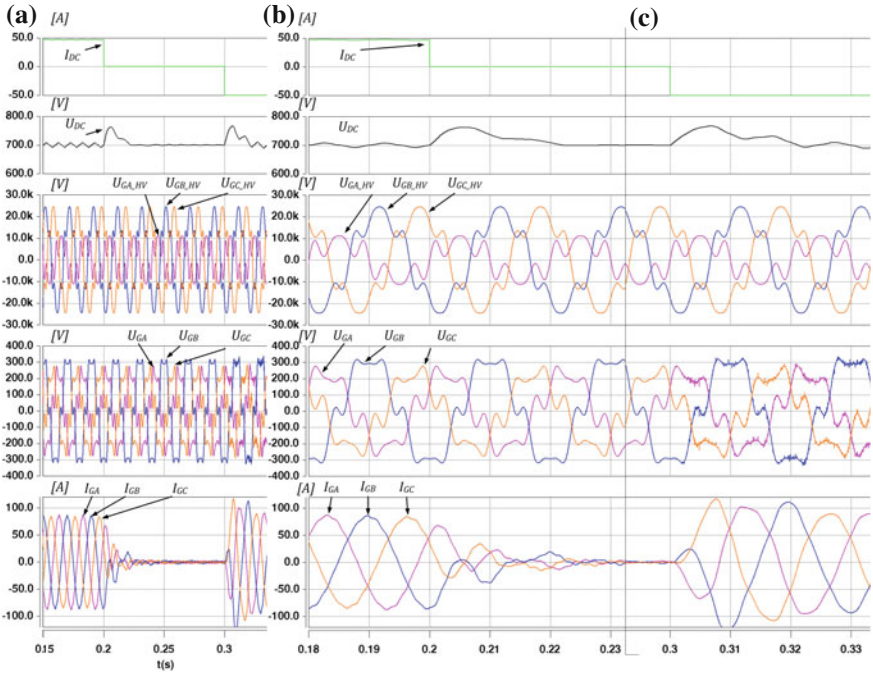

Fig. 36 Operation of 55 kW the GCC with the RDPC-SVM during transients with grid voltage disturbances: dips and harmonics (40 % dip in one phase, 20 % of 5th and 10 % of 7th harmonics. The GCC operation mode transients: **a** from rectifying, to no-load operation and to inverting operation; **b** Zoomed rectifying to no-load operation; **c** Zoomed from no-load to inverting operation. From the *top* I_{DC}—DC-link current (A); U_{DC}—DC-link voltage (V); U_{GA_HV}, U_{GB_HV}, U_{GC_HV}—voltage in high side of the grid transformer (V); U_{GA}, U_{GB}, U_{GC}—voltage in the low side of the transformer (V); I_{GA}, I_{GB}, I_{GC}—phase grid currents (A)

4 Summary and Conclusion

Grid Connected AC-DC Converters (GCC) are used for interfacing distributed energy sources, storages or loads. In recent years there is a strong trend to provide GCCs which assure bidirectional energy flow with as high power quality as possible. To obtain such features of the GCC an advanced control methodology is required. It can be observed an analogy to fast and never ending development of Adjustable Speed Drives (ASD) control methods since last 50 years. In case of ASD researcher wants to obtain the best accuracy, efficiency, dynamic, steady states operation parameters and finally power quality. The list of goals for control methods are rather open and instead to be shorter is longer every years. A control of the GCC can be treated as a dual problem to this defined in case of drives in previous years. Moreover, the important issue in case of the GCC control has to be taken into account i.e. constantly changing and updating an IEC, IEEE, SEMI, or "grid codes" standards and regulations.

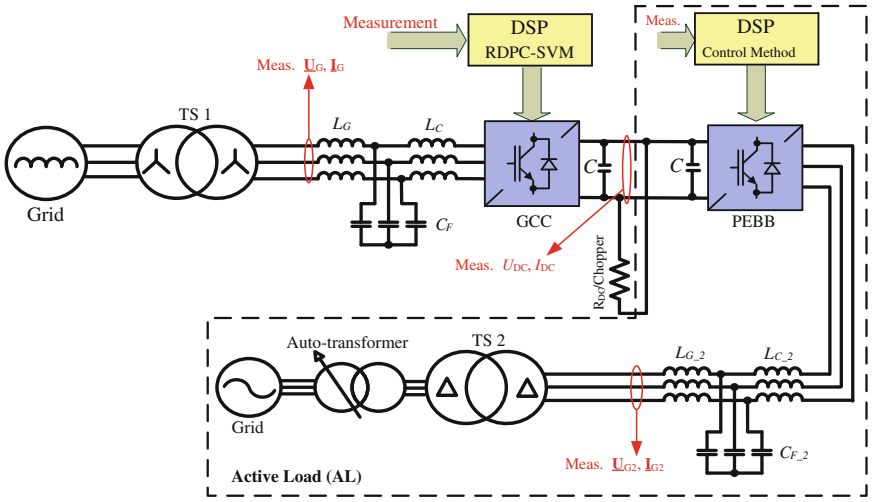

Fig. 37 Configuration of the AC-DC-AC system interconnecting two different voltage sources; model of two different power systems

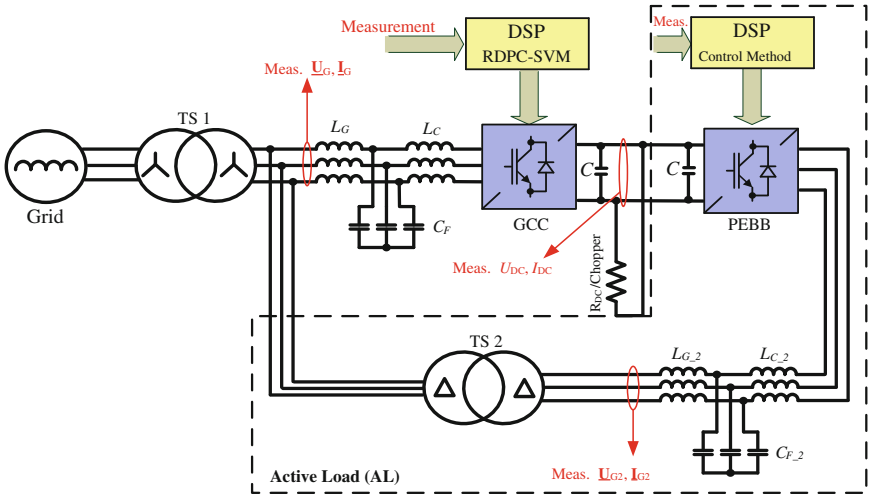

Fig. 38 Configuration of the AC-DC-AC system operating in closed loop of power flow. Setup allows to test the GCC under grid faults with rated power

To fulfill all above mentioned requirements a very flexible software (estimation and control algorithms) has to be developed, tested and implemented. In this chapter the idea of the GCC, treated as Power Electronics Building Block (PEBB) that is unified and ready for programming of different sophisticated functionalities, is given. Authors tried to show that the software (control methods) should be

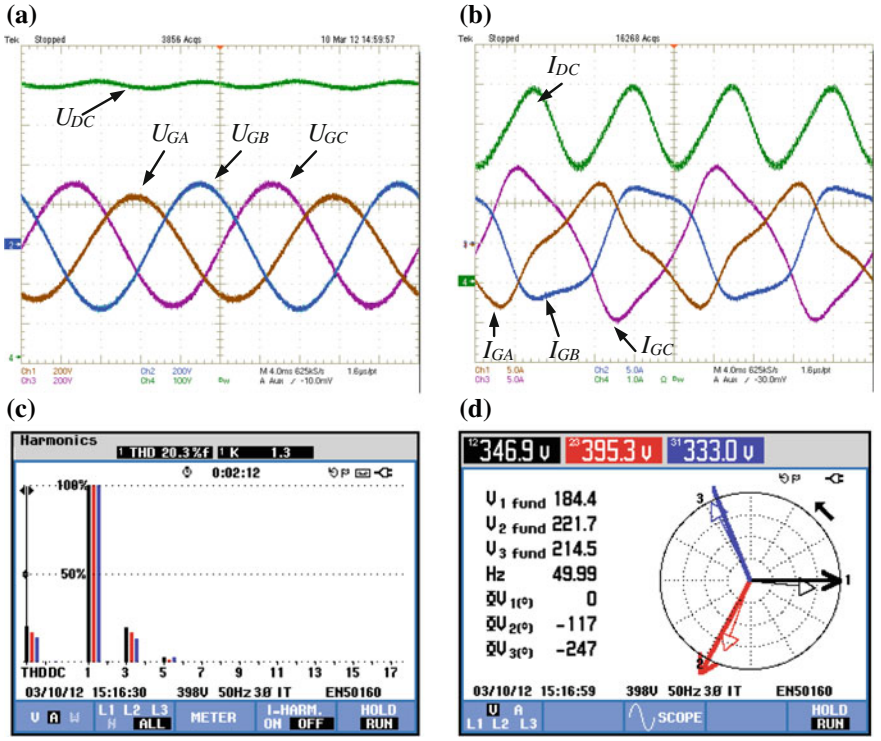

Fig. 39 Operation of the GCC with basic DPC-SVM algorithm under distorted grid voltage conditions (30 % dip in one phase of supplying voltage). **a** U_{AG}, U_{BG}, U_{GC}—grid voltage, U_{DC}—DC-link voltage (V); **b** I_{GA}, I_{GB}, I_{GC}—grid currents, I_{DC}—DC current (A); **c** grid current spectrum and the THD factor (20.3 %); **d** grid voltage and currents vector diagram

designed in modularity way allows to update and add new demanded functions (e.g. dips compensations module, higher harmonics compensation module or standalone operation mode module, etc.). Based on this assumption a new, reliable for grid voltage faults condition control method is proposed: a Robust Direct Power Control with Space Vector Modulation (RDPC-SVM). This control methods joins years of experiences and ideas developed in the research team of prof. Kazmierkowski the Institute of Control and Industrial Electronics, Warsaw University of Technology. The RDPC-SVM is based on generic structure of DPC-SVM extended by implementing several additional control modules assures a new capabilities. Obtained features are verified and tested by simulations and experimental power system [51].

Summarizing, modules of the RDPC-SVM control algorithm gives ability for:

- higher harmonics compensation,
- stable and proper operation even with higher grid impedance,
- stable and proper operation during voltage dips,

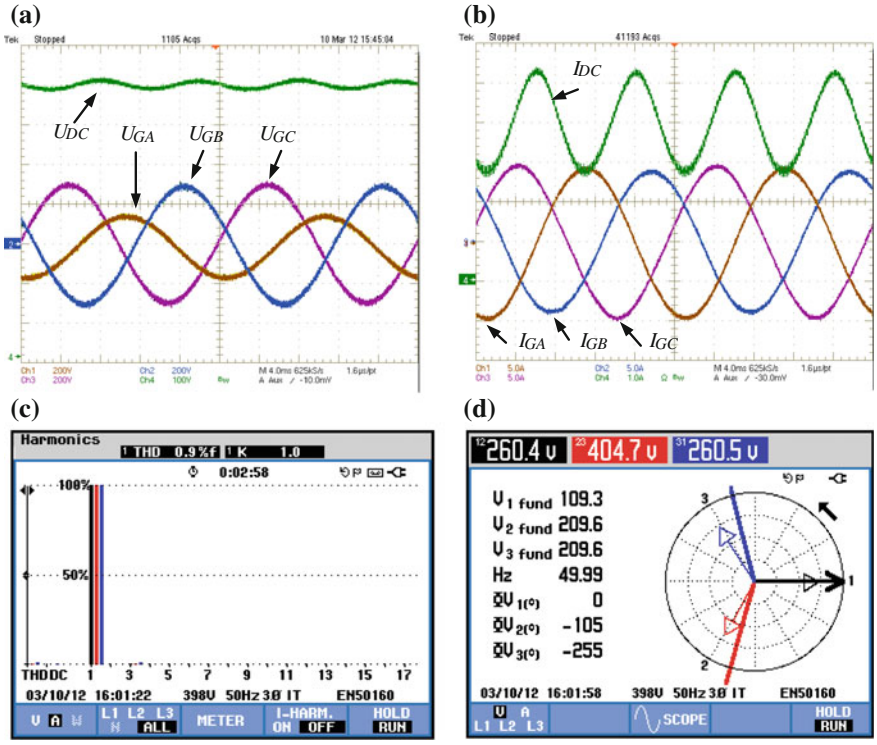

Fig. 40 Operation of the GCC with proposed RDPC-SVM algorithm supplied under distorted grid voltage conditions (50 % dip in one phase of supplying voltage). **a** U_{AG}, U_{BG}, U_{GC}—grid voltage, U_{DC}—DC voltage (V); **b** I_{GA}, I_{GB}, I_{GC}—grid currents, I_{DC}—DC current (A); **c** grid current spectrum and the THD factor (0.9 %); **d** grid voltage and currents vector diagram

- decreased negative impact on the grid voltage, hence reduction of flicker phenomenon (e.g. observed as light blinking) is reduced.

The presented control algorithm is promising for growing number of power electronic converters operating as an interface between the grid and *Renewable Energy Sources* (RES) or *Active Loads* (AL). In the future sustainable AC or DC grids an asymmetrical higher harmonics can appear even more often than symmetrical because the number of single phase loads is higher than three phase loads. Hence, the compensation of asymmetrical harmonics should be taken into account in research process for the GCC. This aspect is not described in the chapter, however, more information can be found in [52]. Moreover, there are many other problems that should be solved in the nearest future by intelligent PEBB.

Authors would like to stress that problems presented in this chapter are just a small part in the field of issues related to integration a GCC with the grid.

The RDPC-SVM control method are going to be used in a TWERD company in Torun, Poland for grid connected converters [101]. It is believed that due to continuous development in power electronics, digital signal processing and intelligent control techniques the newest solution in power electronics will have a strong impact on power quality and reliability improvements in coming decades.

Acknowledgments This work has been partially supported by the National Center for Research and Development, Poland, developing grant no. NR01 0014 06/2009 and also by the European Union in the framework of European Social Fund through the Warsaw University of Technology Development Program, realized by Center for Advanced Studies.

References

1. W. Koczara, Compensation in demand for drive power, in *Proceedings of the PEMC 1990 Conference*, pp. 354–358
2. M.H.J. Bollen, in *Understanding Power Quality Problems—Voltage Sags and Interruptions*. The Institute of Electrical and Electronics Engineers INC (IEEE), Nowy Jork, NY, 10016-5997, John Wiley & Sons Inc (2000)
3. IEEE recommended practice for monitoring electric Power quality, IEEE, Std. 1159-1995, Nowy Jork (1995)
4. IEEE Std 519-1992, IEEE Recommended Practices and Requirements for Harmonic Control in Electrical Power Systems, The Institute of Electrical and Electronics Engineers, Inc., USA (1993)
5. EN 50160, Voltage characteristics of electricity supplied by public electricity networks
6. IEC 61000-2-2 Electromagnetic Compatibility (EMC), Part 2: Environment, Section 2: Compatibility levels for low-frequency conduced disturbances and signaling In public low-voltage Power supply systems
7. IEC 61000-2-4, Electromagnetic compatibility (EMC)—Part 2-4: Environment—Compatibility levels in industrial plants for low-frequency conducted disturbances
8. IEC 61000-3-2 Electromagnetic compatibility (EMC)—Part 3-2: Limits—Limits for harmonic current emissions (equipment input current $\leq$16 A per phase)
9. IEC 61000-3-3, Electromagnetic compatibility (EMC)—Part 3-3: Limits—Limitation of voltage changes, voltage fluctuations and flicker in public low-voltage supply systems, for equipment with rated current $\leq$16 A per phase and not subject to conditional connection
10. IEC 61000-4-7 „Electromagnetic compatibility (EMC)—Part 4-7: Testing and measurement techniques—General guide on harmonics and interharmonics measurements and instrumentation, for power supply systems and equipment connected thereto
11. IEC 61000-4-11, Electromagnetic compatibility (EMC)—Part 4-11: Testing and measurement techniques—Voltage dips, short interruptions and voltage variations immunity tests
12. IEC 61000-4-14, Electromagnetic compatibility (EMC)—Part 4-14: Testing and measurement techniques—Voltage fluctuation immunity test for equipment with input current not exceeding 16 A per phase
13. IEC 61000-4-15, Electromagnetic compatibility (EMC)—Part 4-15: Testing and measurement techniques—Flickermeter—Functional and design specifications
14. SEMI F47-0706 Specification for Semiconductor Processing Equipment Voltage Sag Immunity
15. PSE Operator S.A., IRiESP—operational instruction in power distribution systems (in Polish)

16. J.A. Oliver, R. Lawrence, B.B. Banerjee, How to specify power-quality-tolerant process equipment, in *IEEE Industrial Applications Magazine*, September/October 2002, pp. 21–30
17. Planing levels for harmonic voltages, Engineering Recommendation G5/4-1
18. V. Ajodhia, B. Franken, in *Regulation of Voltage Quality* (Kema Consulting, Bonn, 2007)
19. R. Strzelecki, G. Benysek, in *Power Electronics in Smart Electrical Energy Networks* (Springer, Berlin, 2008), p. 414
20. M. Jasinski, M.P. Kazmierkowski, H.Ch. Soerensen, E. Friis-Madsen, Direct power and torque control of AC/DC/AC converter-generator subset in wave-to-wire power train for renewable energy system-wave dragon MW. WSEAS Trans. Power Syst. **1**(10), 1681–1688, October 2006, ISSN1790-5060
21. J.W. Kolar, H. Ertl, K. Edelmoser, F.C. Zach, Analysis of the control behavior of a bidirectional three-phase PWM rectifier system, in *Proceedings of the EPE 1991 Conference*, 1991, pp. (2-095)–(2-100)
22. J.A. Oliver, R. Lawrence, B.B. Banerjee, How to specify power-quality-tolerant process equipment, IEEE Industrial Applications Magazine, September/October 2002, pp. 21–30
23. N. Mohan, T.M. Undeland, W.P. Robbins, in *Power Electronics: Converters, Applications, and Design* (Wiley, New York, 1989), p. 667
24. F. Abrahamsen, A. David, Adjustable speed drive with active filtering capability for harmonic current compensation, in *Proceedings of the PESC 1995 Conference*, pp. 1137–1143
25. H. Akagi, New trends in active filters for power conditioning. IEEE Trans. Ind. Appl. **32**, 1312–1332 (1996)
26. M. Cichowlas, PWM Rectifier with Active Filtering, Warsaw University of Technology, Ph.D. Thesis, Warsaw, Poland, 2004
27. D. Zhou, D. Rouaud, Regulation and design issues of a PWM three-phase rectifier, in *Proceedings of the 25th Annual Conference on IECON'99*, vol. 1, pp. 485–489 (1999)
28. S. Piasecki, M. Jasinski, A. Milicua, Brief view on control of grid-interfacing AC-DC-AC converter and active filter under unbalanced and distorted voltage conditions, Int. J. Comput. Math. Electr. Electron. Eng. (COMPEL) on EVER'09, Emerald **30**(1), 351–373 (2011)
29. V. Blasko, V. Kaura, A new mathematical model and control of a tree-phase AC-DC voltage source converter. IEEE Trans. Power Electron. **12**(1), 116–123 (1997)
30. R.P. Burgos, E.P. Wiechmann, J. Holtz, Complex state variables modeling and nonlinear control of PWM voltage- and current-source rectifiers, in *28th Annual Conference on IECON 02, Industrial Electronics Society, IEEE 2002*, Vol. 1, 5–8 Nov. 2002, pp. 187–192
31. G.F. Franklin, J. David Powell, A. Emami-Naeini, in *Feedback Control of Dynamic Systems,* 3rd edn (Addison-Wesley, Reading, 1994)
32. M. Malinowski, M. Jasinski, M.P. Kazmierkowski, Simple direct power control of three-phase PWM rectifier using space-vector modulation (DPC-SVM). IEEE Trans. Ind. Electron. **51**(2), 447–454 (2004)
33. Spagnuolo, G., Petrone, G., Araujo, S.V., Cecati, C., Friis-Madsen, E., Gubia, E., Hissel, D., Jasinski, M., Knapp, W., Liserre, M., Rodriguez, P., Teodorescu, R., Zacharias, P., Renewable energy operation and conversion schemes: a summary of discussions during the seminar on renewable energy systems. IEEE Ind. Electron. Mag. **4**(1), 38–51 (2010)
34. G. Joos, N.R. Zargari, P.D. Ziogas, A new class of current-controlled suppressed-link ac to ac frequency changers, in *Proceedings of Power Electronics Specialists Conference, 22nd Annual IEEE*, 24–27 June 1991, pp. 830–837
35. M.P. Kazmierkowski, L. Malesani, Current control techniques for three-phase voltage-source PWM converters: a survey. IEEE Trans. Ind. Electron **45**(5), 691–703 (1998)
36. B.-K. Lee, M. Ehsani, A simplified functional simulation model for three-phase voltage-source inverter using switching function concept. IEEE Trans. Ind. Electron. **48**(2), 209–321 (2001)

37. H. Mao, D. Boroyevich, F.C.Y. Lee, Novel reduced-order small-signal model of a three-phase PWM rectifier and its application in control design and system analysis. IEEE Trans. Power Electron. **13**(3), 511–521 (1998)
38. E.P. Weichmann, P.D. Ziogas, V.R. Stefanovic, Generalized functional model for three-phase PWM inverter/rectifier converters, IEEE Trans. Ind. Appl. **IA-23**(2), 236–246, (1987)
39. R. Wu, S.B. Dewan, G.L. Slemon, Analysis of a PWM AC to DC voltage source converter under the predicted current control with fixed switching frequency. IEEE Trans. Ind. Appl. **27**(4), 756–764 (1991)
40. R. Wu, S.B. Dewan, G.R. Slemon, A PWM AC-to-DC converter with fixed switching frequency, IEEE Trans. Ind, Appl. **26**(5), 880–885, (1990)
41. R. Wu, S.B. Dewan, G.R. Slemon, Analysis of an ac-to-dc voltage source converter using PWM with phase and amplitude control. IEEE Trans. Ind. Appl. **27**(2), 355–364 (1991)
42. K. Xing, F.C. Lee, J.S. Lai, Y. Gurjit, D. Borojevic, Adjustable speed drive neutral voltage shift and grounding issues in a DC distributed system, in *Proceedings of the Annual Meeting of the IEEE-IAS*, 1997, pp. 517–524
43. Y. Xue, X. Xu, T.G. Habatler, D.M. Divan, A low cost stator flux oriented voltage source variable speed drive, in *Industry Applications Society Annual Meeting, 1990., Conference Record of the 1990 IEEE*, 7–12 Oct. 1990, pp. 410–415
44. N.R. Zargari, G. Joós, Performance investigation of a current-controlled voltage-regulated PWM rectifier in rotating and stationary frames. IEEE Trans. Ind. Electron. **42**(4), 396–401 (1995)
45. M. Malinowski, Sensorless Control Strategies for Three-Phase PWM Rectifiers, Warsaw University of Technology, Ph.D. Thesis, Warszawa, 2001
46. M. Liserre, Innovative control techniques of power converters for industrial automation, Politecnico di Bari, Ph.D. Thesis, Italy, 2001
47. P. Rodriguez, R. Teodorescu, I. Candela, A.V. Timbus, M. Liserre, F. Blaabjerg, New positive-sequence voltage detector for grid synchronization of power converters under faulty grid conditions, in *Power Electronics Specialists Conference, 2006. PESC '06. 37th IEEE*, pp. 1–7, 18–22 June 2006
48. M. Jasinski, Direct power and torque control of AC-DC-AC converter-fed induction motor drives, Ph.D. Thesis, Warsaw University of Technology, Warsaw, Poland, 2005
49. M.P. Kazmierkowski, H. Tunia, *Automatic Control of Converter-Fed Drives* (Elsevier, Amsterdam, 1994), p. 559
50. K. Mikołajuk, Principles of Power Electronics Circuits, Wydawnictwo Naukowe PWN, 1998, p. 525, (in Polish)
51. S. Piasecki, M. Jasinski, G. Wrona, W. Chmielak, Robust Control of Grid Connected AC-DC Converter for Distributed Generation, in *IECON 2012*, Montreal, Canada, pp. 5844–5849
52. G. Wrona, M. Jasinski, Asymmetrical Higher harmonics compensation in grid connected AC-DC converter control, in *13th International Symposium Typical Problems in the Field of Electrical and Power Engineering*, Doctoral School of Energy and Geotechnology II, Parnu, Estonia 14-19.01.2013, pp. 126–131. ISBN978-9985-69-054-3
53. A. Sikorski, Problems related with switching loses minimization in PWM AC/DC/AC fed induction machine, Politechnika Białostocka, Rozprawy Naukowe nr. 58, Białystok 1998, p. 217 (in Polish)
54. A. Sikorski, Current control conditions control for AC/DC, Nonsinusoidal Currents, EPN' 2000, Zielona Gora, 2000 (in Polish)
55. K. Jalili, Investigation of Control Concepts for High-Speed Induction Machine Drives and Grid Side Pulse-Width Modulation Voltage Source Converters, PhD Thesis, Technischen Universität Dresden, p. 174, 2009
56. M. Liserre, F. Blaabjerg, A. Dell'Aquila, Step-by-step design procedure for a grid-connected three-phase PWM voltage source converter. Int. J. Electron. **91**(8), 445–460 (2004)

57. M. Liserre, A. Dell'Aquila, F. Blaabjerg, Genetic algorithm-based design of the active damping for an LCL-filter three-phase active rectifier. IEEE Trans. Power Electron. **19**(1), 76–86 (2004)
58. M. Liserre, A. Dell'Aquila, F. Blaabjerg, Stability improvements of an LCL-filter based three-phase active rectifier, IEEE, 2002, pp. 1195–1201
59. K.A. Rothenhagen, M. Jasinski, M.P. Kazmierkowski, Grid connection of multi-megawatt clean wave energy power plant under weak grid condition, in *EPE-PEMC'08*, 1–3 September 2008, Poznan, Poland, on CD
60. EPCOS, Aluminium Electrolic Capacitors-Genera Technical Information, DataSheet, www.epcos.com
61. EPCOS, Aluminium Electrolic Capacitors-Applications, DataSheet, www.epcos.com
62. D.G. Holmes, T.A. Lipo, *Pulse Width Modulation for Power Converters, Principles and Practice* (Wiley-Interscience and IEEE Press, New York, 2003)
63. M. Alakula, J.E. Persson, Vector controlled ac/ac converters with a minimum of energy storage, in *Proceedings of the IEEE Conference*, 1994, pp. 1130–1134
64. M.M. Bech, F. Blaabjerg, J.-K. Pedersen, Random modulation techniques with fixed switching frequency for three-phase power converters. IEEE Trans. Power Electron. **15**(4), 753–761 (2000)
65. V. Blasko, Analysis of a hybrid PWM based on modified space-vector and triangle-comparison methods, IEEE Trans. Ind. Appl. **33**(3), 756–764 (1997)
66. A. Boglietti, G. Griva, M. Pasterelli, F. Profumo, T. Adam, Different PWM modulation techniques indexes performance evaluation, in *Proceedings of the IEEE Conference*, 1993, pp.193–199
67. A.M. Hava, S.-K. Sul, R.J. Kerkman, Dynamic overmodulation characteristics of triangle intersection PWM methods. IEEE Trans. Ind. Appl. **35**(4), 896–907 (1999)
68. A.M. Hava, R.J. Karkman, T.A. Lipo, A high-performance generalized discontinuous PWM algorithm. IEEE Trans. Ind. Appl. **34**(5), 059–1071 (1998)
69. J.W. Kolar, H. Ertl, F.C. Zach, Influence of the modulation method on the conduction and switching losses of a PWM converter system. IEEE Trans. Ind. Appl. **27**(6), 1063–1075 (1991)
70. D.-C. Lee, G.-M. Lee, A novel overmodulation technique for space-vector PWM inverters. IEEE Trans. Power Electron. **13**(6), 1144–1151 (1998)
71. H.W. Van Der Broeck, H.C. Skudelny, Analysis and realization of a pulsewidth modulator based on voltage space vectors. IEEE Trans. Ind. Appl. **24**(1), 142–150 (1988)
72. M. Winkelnkemper, S. Bernet, Design and optimalization of the DC-link capacitor of PWM voltage source inverter with active frontend for low-voltage drives, in *Proceedings of the EPE 2003 Conference*, 2003
73. A. Carlsson, The back-to-back converter control and design, Lund Institute of Technology, Ph.D. Thesis, Lund, 1998
74. L. Moran, P.D. Ziogas, G. Joos, Design aspects of synchronous PWM rectifier-inverter systems under unbalanced input voltage conditions. IEEE Trans. Ind. Appl. **28**(6), 1286–1293 (1992)
75. B.K. Bose, *Modern Power Electronics and AC Drives* (Prentice-Hall, Upper Saddle River, 2002)
76. B.T. Ooi, J.W. Dixon, A.B. Kulkarni, M. Nishimoto, An integrated AC drive system using a controlled-current PWM Rectifier/Inverter link. IEEE Trans. Power Electron. **3**(1), 64–71 (1988)
77. P. Cortes, J. Rodriguez, P. Antoniewicz, M. Kazmierkowski, Direct power control of an AFE using predictive control. IEEE Trans. Power Electron. **23**(5), 2516–2523 (2008)
78. J.C.R. Martinez, R. Kennel, A.L. Sheakh Ameen, Comparative analysis of on-line and off-line explicit solutions, applied in predictive direct current, in *5th IET International Conference on Power Electronics, Machines and Drives (PEMD 2010)*, April 2010, pp.1,6, 19–21

79. M. Liserre, C. Klumpner, F. Blaabjerg, V.G. Monopoli, A. Dell'Aquila, Evaluation of the ride-through capability of an active-front-end adjustable speed drive under real grid conditions, in *Proceedings of the Annual Conference of the IEEE-IES*, 2004
80. M. Liserre, F. Blaabjerg, S. Hansen, Design and control of an LCL-filter based three-phase active rectifier. IEEE Trans. Ind. Appl. **41**(5), 1281–1291 (2005)
81. J.A. Suul, A. Luna, P. Rodriguez, T. Undeland, Voltage-sensor-less synchronization to unbalanced grids by frequency-adaptive virtual flux estimation. IEEE Trans. Ind. Electron. **59**(7), 2910–2923 (2012)
82. N. Zaveri, A. Mehta, A. Chudasama, Performance analysis of various SRF methods in three phase shunt active filters, in *2009 International Conference. on Industrial and Information Systems (ICIIS),* pp. 442–447, 28–31 Dec. 2009
83. R. Teodorescu, F. Blaabjerg, M. Liserre, P.C. Loh, Proportional resonant controllers and filters for grid-connected voltage-source converters. IEE Proc. Eletr. Power Appl. **153**(5), 750–762 (2006)
84. H. Song, K. Nam, Dual current control scheme for PWM converter under unbalanced input voltage conditions. IEEE Trans. Energy Conv. **46**(5), October 1999
85. R. Teodorescu, M. Liserre, P. Rodríguez, *Grid Converters for Photovoltaic and Wind Power Systems* (Wiley-IEEE, New York, 2011), p. 416
86. M.P. Kaźmierkowski, M. Jasiński, Power electronic grid-interface for renewable ocean wave energy, in *International Conference-Workshop Compatibility and Power Electronics*, 1–3 June 2011-CPE 2011, Tallinn, Estonia, pp. 457–463
87. M. Jasinski, K. Rafal, M. Bobrowska-Rafal, S. Piasecki, Grid interfacing of distributed energy sources by three-level BtB NPC converter under distorted grid voltage, in *2011 Workshop on Predictive Control of Electrical Drives and Power Electronics (PRECEDE)*, pp. 30–35, 14–15 Oct. 2011
88. G.D. Marques, J.F. Silva, Direct voltage control of a PWM AC/DC voltage converter, in *Proceedings of the EPE 1997 Conference*, 1997, pp. (3.222)–(3.227)
89. H. Hur, J. Jung, K. Nam, A fast dynamics DC-link power-balancing scheme for a PWM converter-inverter system. IEEE Trans. Ind. Electron. **48**(4), 794–803 (2001)
90. J. Jung, S. Lim, K. Nam, A feedback linearizing control scheme for a PWM converter-inverter having a very small DC-link capacitor. IEEE Trans. Ind. Appl. **35**(5), 1124–1131 (1999)
91. F. Kamran, T.G. Habatler, An improved deadbeat rectifier regulator using a neural net predictor. IEEE Trans. Power Electron. **10**(4), 504–510 (1995)
92. D.-C. Lee, K.-D. Lee, G- M. Lee, Voltage control of PWM converters using Feedback Linearization, in *Proceedings of Thirty-Third IAS Annual Meeting. The 1998 IEEE*, Vol. 2, 12–15 Oct. 1998, pp. 1491–1496
93. M.P. Kazmierkowski, R. Krishnan, F. Blaabjerg (Eds.), in *Control in Power Electronics* (Academic Press, New York, 2002), p. 579
94. R. Ottersten, J. Svensson, Vector current controlled voltage source converter-deadbeat control and saturation strategies. IEEE Trans. Power Electron. **17**(2), 279–285 (2002)
95. T. Ohnishi, Three-phase PWM converter/inverter by means of instantaneous active and reactive power control, in *Proceedings of the IEEE-IECON Conference*, 1991, pp. 819–824
96. V. Manninen, Application of direct torque control modulation technology to a line converter, in *Proceedings of the EPE 1995 Conference,* 1995, pp. 1.292–1.296
97. T. Noguchi, H. Tomiki, S. Kondo, I. Takahashi, Direct power control of PWM converter without power-source voltage sensors. IEEE Trans. Ind. Appl. **34**(3), 473–479 (1998)
98. H. Kim, H. Akagi, The instantaneous power theory on the rotating p-q-r reference frames, in *Proceedings of the IEEE 1999 International Conference on Power Electronics and Drive Systems, 1999. PEDS '99*, Vol. 1, 27–29 July 1999, pp. 422–427
99. J. Holtz, Pulsewidth modulation for electronics power conversion. Proc. IEEE **82**(8), 1194–1214 (1994)

100. M. Malinowski, M.P. Kazmierkowski, M. Jasiński, Virtual flux based direct power control of tree-phase PWM rectifiers, Electrical Power Quality and Utilization, Vol. VII, Sheet 1, 2001, pp. 129–138
101. www.twerd.pl
102. G.E. Dullerud, F.G. Paganini, *A course in robust control theory a convex approach*, University of Illinois Urbana-Champaign and University of California Los Angeles, Springer, 2005, p. 383
103. www.nowaplus.com.pl